ANNUAL REVIEWS

Annual Review of Biophysics

Interaction Dynamics of Intrinsically Disordered Proteins from Single-Molecule Spectroscopy

Aritra Chowdhury,[1] Daniel Nettels,[1] and Benjamin Schuler[1,2]

[1]Department of Biochemistry, University of Zurich, Zurich, Switzerland; email: a.chowdhury@bioc.uzh.ch, nettels@bioc.uzh.ch, schuler@bioc.uzh.ch

[2]Department of Physics, University of Zurich, Zurich, Switzerland

Annu. Rev. Biophys. 2023. 52:433–62

First published as a Review in Advance on February 7, 2023

The *Annual Review of Biophysics* is online at biophys.annualreviews.org

https://doi.org/10.1146/annurev-biophys-101122-071930

Keywords

protein binding, single-molecule Förster resonance energy transfer, single-molecule FRET, disordered complexes, kinetics, molecular simulations

Abstract

Many proteins contain large structurally disordered regions or are entirely disordered under physiological conditions. The functions of these intrinsically disordered proteins (IDPs) often involve interactions with other biomolecules. An important emerging effort has thus been to identify the molecular mechanisms of IDP interactions and how they differ from the textbook notions of biomolecular binding for folded proteins. In this review, we summarize how the versatile tool kit of single-molecule fluorescence spectroscopy can aid the investigation of these conformationally heterogeneous and highly dynamic molecular systems. We discuss the experimental observables that can be employed and how they enable IDP complexes to be probed on timescales from nanoseconds to hours. Key insights include the diverse structural and dynamic properties of bound IDPs and the kinetic mechanisms facilitated by disorder, such as fly-casting; disorder-mediated encounter complexes; and competitive substitution via ternary complexes, which enables rapid dissociation even for high-affinity complexes. We also discuss emerging links to aggregation, liquid–liquid phase separation, and cellular processes, as well as current technical advances to further expand the scope of single-molecule spectroscopy.

Contents

INTRODUCTION

Many proteins contain large regions that do not form a well-defined tertiary structure under physiological conditions, and some are even entirely disordered. In the human proteome, for example, >40% of all proteins are predicted to contain disordered regions longer than 30 amino acid residues, and approximately 5% of all proteins are predicted to be fully disordered (≥95% disordered residues) (112, 160, 162). These intrinsically disordered proteins (IDPs) have been investigated with a broad range of methods, especially nuclear magnetic resonance (NMR) spectroscopy (25, 40, 104), small-angle X-ray scattering (SAXS) (77), electron paramagnetic resonance (EPR) spectroscopy (165), and single-molecule fluorescence spectroscopy (99, 107, 134), often using integrative approaches in combination with molecular simulations (18, 132, 140), and in some cases even in live cells (123). Owing to these efforts, we now have an increasingly detailed picture of IDPs, in terms of both their structural and dynamic properties.

An important next step is to relate these properties to the cellular functions of IDPs. The full range of IDP functions is only starting to be revealed (5, 34), but it is evident that disordered proteins or regions often bind other biological macromolecules. IDPs commonly interact with many different binding partners and can thus function as interaction hubs in cellular communication and regulation networks (114, 169). A famous example is the tumor suppressor p53, which can bind to more than a hundred different proteins via its disordered regions (114). Remarkably detailed information on some IDP binding processes has been obtained in individual cases, especially for examples of coupled folding and binding, where a well-defined three-dimensional structure forms in the complex (168). However, our understanding of IDP interactions in general is still fragmentary.

A key insight has been that a broad spectrum of disorder can be present in the complexes of IDPs with other proteins or nucleic acids (13, 48, 49, 132, 158). For protein–protein complexes, for example, the spectrum of disorder ranges from the classical textbook examples of fully folded proteins that bind to each other via well-defined interfaces with complementary shapes and interaction patterns all the way to complexes between two IDPs that fully retain their disorder in

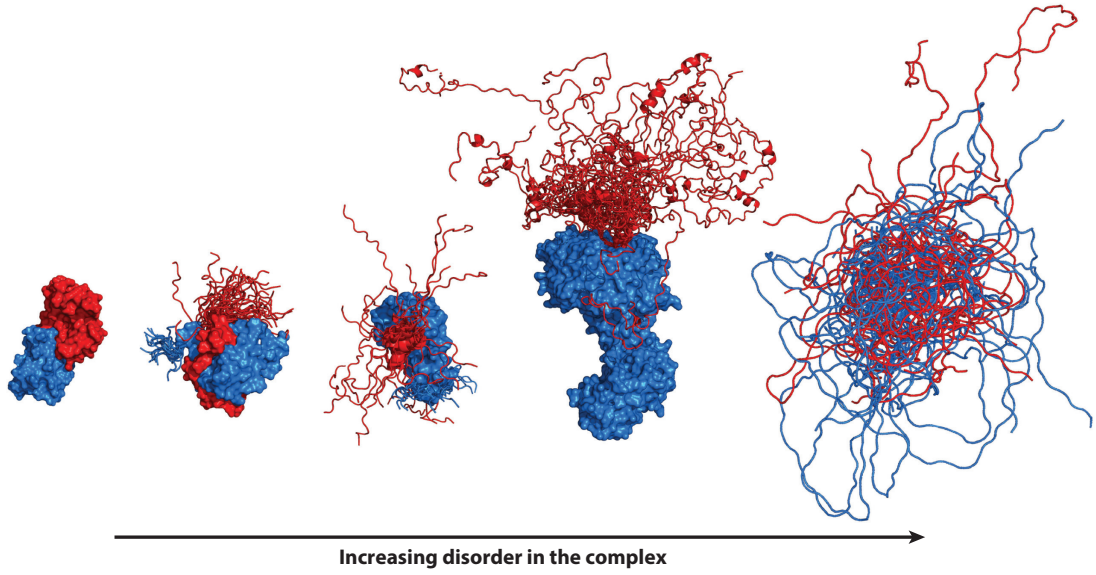

Figure 1

The spectrum of disorder in protein complexes. Proteins retain various degrees of disorder in their bound states (158), as illustrated with the following examples (from left to right, with the first protein mentioned in the complex colored in red and the second in blue): Colicin E9 with Im9 (PDB 1EMV); RelA-TAD/CBP-TAZ1 complex (PDB 2LWW); Gcn4 activation domain bound to the mediator coactivator domain 1 of Gal11/med15 (PDB 2LPB); complex of Sic1 with the Cdc4 subunit of ubiquitin ligase (105); complex of ProTα and H1 [ensemble from coarse-grained simulations based on single-molecule FRET data (16)]. Stably folded proteins or domains are shown in surface representation; disordered regions are shown in schematic representation, with multiple conformations from NMR or modeled ensembles overlaid. Figure adapted from Reference 132 with permission from Elsevier. Abbreviations: FRET, Förster resonance energy transfer; NMR, nuclear magnetic resonance; PDB, Protein Data Bank.

the bound state (**Figure 1**). Intermediate cases include complexes that are largely structured with only small disordered tails or loops; complexes where binding is mediated by a folded segment, such as an α-helix, with the remainder of the protein remaining disordered; and complexes where a folded protein binds one or multiple short sequence motifs of an IDP that stays otherwise fully disordered. Two of the central challenges are now (*a*) to characterize the structural and dynamic properties of these disordered complexes and (*b*) to elucidate the mechanistic implications for binding, especially whether and how the binding mechanisms of IDPs differ from those of folded proteins, and in what cases they go beyond established paradigms.

The lack of well-defined tertiary structure entails an obvious challenge for characterizing IDP complexes. Some of the most powerful methods for determining the three-dimensional structures of folded proteins, such as X-ray crystallography and cryo-electron microscopy, provide little, if any, information about disordered regions. As in the case of individual IDPs in isolation, we thus need to employ techniques that are suitable for probing the structurally heterogeneous ensembles of disordered complexes. A closely related challenge is the rapid dynamics of disordered regions and of larger assemblies composed of both folded and disordered parts. Arguably the most versatile experimental methods for investigating both the structural and dynamic properties of such heterogeneous ensembles are single-molecule spectroscopy, especially single-molecule Förster resonance energy transfer (FRET), and NMR. The use of both techniques for IDPs in general has been summarized in several recent reviews (25, 40, 55, 99, 107, 115, 134). In this review, we focus specifically on advances in single-molecule fluorescence spectroscopy for probing the dynamics

Disordered complexes: protein complexes in which at least one binding partner retains some disorder in the bound state

of IDPs within their complexes, the resulting interaction kinetics, and the use of time-resolved information for elucidating the mechanisms of target binding.

MONITORING IDP BINDING WITH SINGLE-MOLECULE FRET SPECTROSCOPY

Monitoring a binding reaction requires a concomitant change in experimental observables. We thus briefly summarize the information from single-molecule fluorescence measurements that can be employed for investigating the interactions of IDPs (**Figure 2**), for which we assume a basic understanding of single-molecule spectroscopy and FRET (86, 91, 130, 136) on the part of the reader. The most sensitive observable in single-molecule FRET experiments is usually a change in intra- or intermolecular transfer efficiency, E, based on the classical use of single-molecule FRET as a spectroscopic ruler (133, 151) (**Figure 2*a***). Given the known distance dependence of energy transfer from Förster's theory (47), measurements of E can be used to infer interdye distances or distance changes. A distance change of 1 Å close to a typical Förster radius of 5.4 nm, for instance, leads to a change in transfer efficiency of approximately 0.03, which is reliably detectable in high-quality measurements.[1] However, many interactions of IDPs are accompanied by much larger distance changes, resulting in pronounced shifts in transfer efficiency (**Figure 3**).

In confocal single-molecule fluorescence instruments, the use of multiple laser sources and detection channels for different wavelength ranges and polarizations, as well as the detection based on time-correlated single-photon counting, yields useful information beyond the commonly available donor and acceptor emission intensities (75, 85, 134, 142) (**Figure 2**). Examples of particularly valuable observables for monitoring IDP interactions are fluorescence anisotropy (**Figure 2*b***), fluorescence lifetimes (**Figure 2*c*,*d***), stoichiometry (**Figure 2*f***), and the relaxation times and amplitudes from fluorescence correlation spectroscopy (FCS) (**Figure 2*e***) (134). In multiparameter recordings, all of these quantities can be extracted from the same measurement. Experiments can be performed either on molecules freely diffusing in solution or on molecules that are surface-immobilized. Free-diffusion experiments provide good statistics from thousands of molecules, but the maximum observation time for each molecule is limited to approximately a millisecond by its translational diffusion through the confocal volume. Surface experiments enable observation times of minutes (limited by photobleaching). Confocal measurements require the individual molecules to be recorded sequentially, which limits throughput. Camera-based wide-field imaging methods (usually in combination with total internal reflection fluorescence) (72, 88) allow many molecules to be recorded simultaneously and thus enable greater throughput, but time resolution is usually limited to the millisecond range by the frame rates of sufficiently sensitive cameras, and the lack of time-correlated single-photon counting reduces spectroscopic versatility.

Experiments using alternating excitation of donor and acceptor (75, 85) can reveal the stoichiometry in intermolecular FRET measurements where one binding partner carries the donor and the other carries the acceptor (**Figure 2*f***). Binding in such cases is monitored either by the appearance of FRET or by the colocalization of donor and acceptor signals.[2] Alternating excitation further enables the spectroscopic identification of molecules that do not contain both an active

[1]The typical accuracy of single-molecule measurements of FRET efficiency has been estimated to be approximately 0.04 in a benchmark study (61). The precision, however, is much higher, and relative changes in transfer efficiency of less than 0.01 can be measured reliably with sufficient data acquisition statistics and stable instrumentation (81).

[2]Note, however, that intermolecular single-molecule FRET experiments are usually limited to high-affinity interactions ($K_d \lesssim 10$ nM), since the labeled molecules can only be present at concentrations that are low enough to keep the background sufficiently low for single-molecule detection. In intramolecular FRET

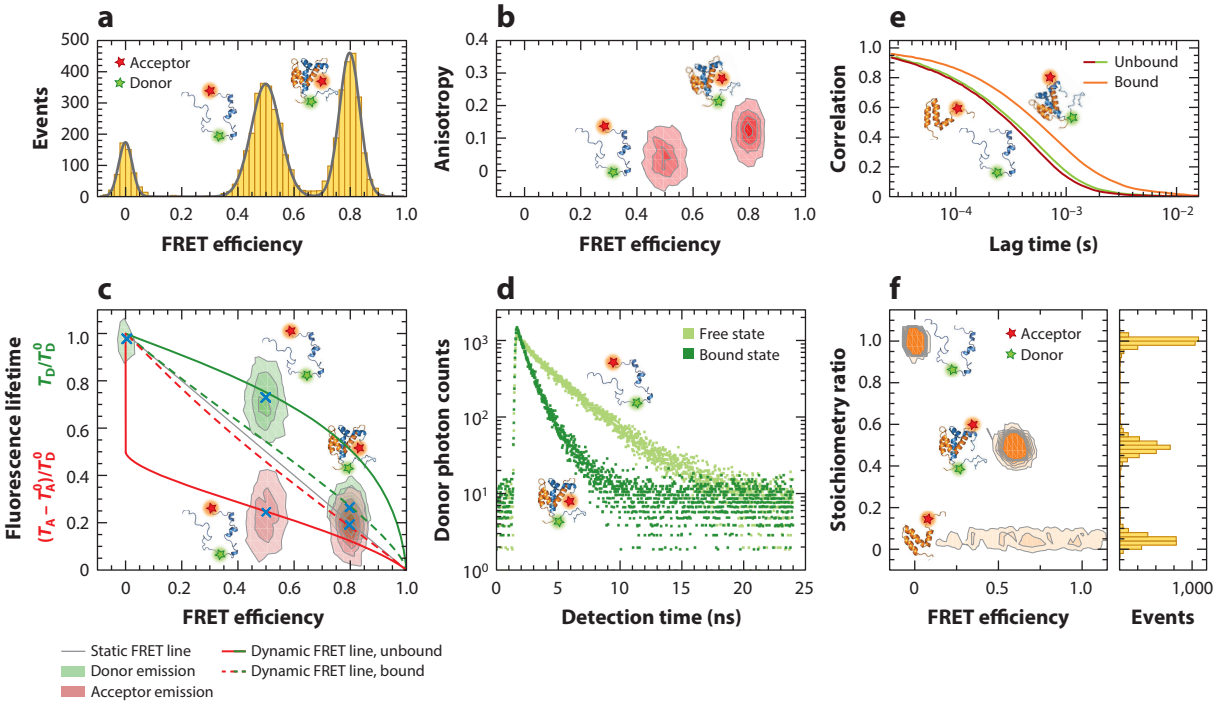

Figure 2

Observables for monitoring protein binding with single-molecule fluorescence spectroscopy. Examples of observables from multiparameter single-molecule fluorescence detection of freely diffusing molecules are illustrated for (*a–d*) intramolecular and (*e*, *f*) intermolecular FRET measurements of the interaction between two IDPs labeled with donor (*green*) and acceptor (*red*), as indicated in the schematics in each panel. (*a*) FRET efficiency (*E*) reports on changes in interdye distance, and thus conformation, upon binding. The peak at $E = 0$ is from molecules lacking an active acceptor dye. (*b*) Fluorescence anisotropy reports on changes in rotational mobility of the fluorophores upon binding, in this case for direct acceptor excitation. (*c*) Deviations from the static FRET line (*gray*) in fluorescence lifetime (donor emission in green, acceptor emission in red) versus FRET efficiency diagrams (29, 58, 73, 134) report on the presence of a rapidly sampled distance distribution, in this case in the unbound state represented by a polymer model (*solid lines*). Residual deviations from the static FRET line in the bound state (*dashed lines*) originate from dye and linker flexibility. (*d*) Subpopulation-specific fluorescence lifetime decays (in this case for the donor) provide an orthogonal way of assessing differences in FRET efficiency between free (*light green*) and bound (*dark green*) states. (*e*) Changes in translational diffusion times through the confocal volume upon binding and the concentrations of labeled species are available from FCS (unbound in green and red; bound in orange). (*f*) The stoichiometry of complexes in intermolecular FRET experiments can be assessed by alternating or pulsed interleaved donor and acceptor excitation (75, 85). A stoichiometry ratio of $S = 1$ corresponds to donor-labeled molecules, $S = 0.5$ corresponds to the 1:1 complex, and $S = 0$ corresponds to acceptor-labeled molecules. All examples are from simulations of photon emission and translational diffusion performed with Fretica (**https://schuler.bioc.uzh.ch/programs**) using experimentally realistic parameters. Abbreviations: FCS, fluorescence correlation spectroscopy; FRET, Förster resonance energy transfer; IDP, intrinsically disordered protein.

donor and an acceptor dye in intramolecular measurements, and it greatly aids in the instrument calibration required for extracting accurate distance information (61, 68, 85, 89). Fluorescence anisotropy allows us to assess the rotational freedom of the fluorophores and to quantify rotational

experiments, in contrast, the unlabeled binding partner can be added at much higher concentrations. Single-molecule measurements at higher concentrations of fluorescently labeled species (into the micromolar range) are made possible by reducing the size of the observation volume, for example, with zero-mode waveguides (35, 111, 175).

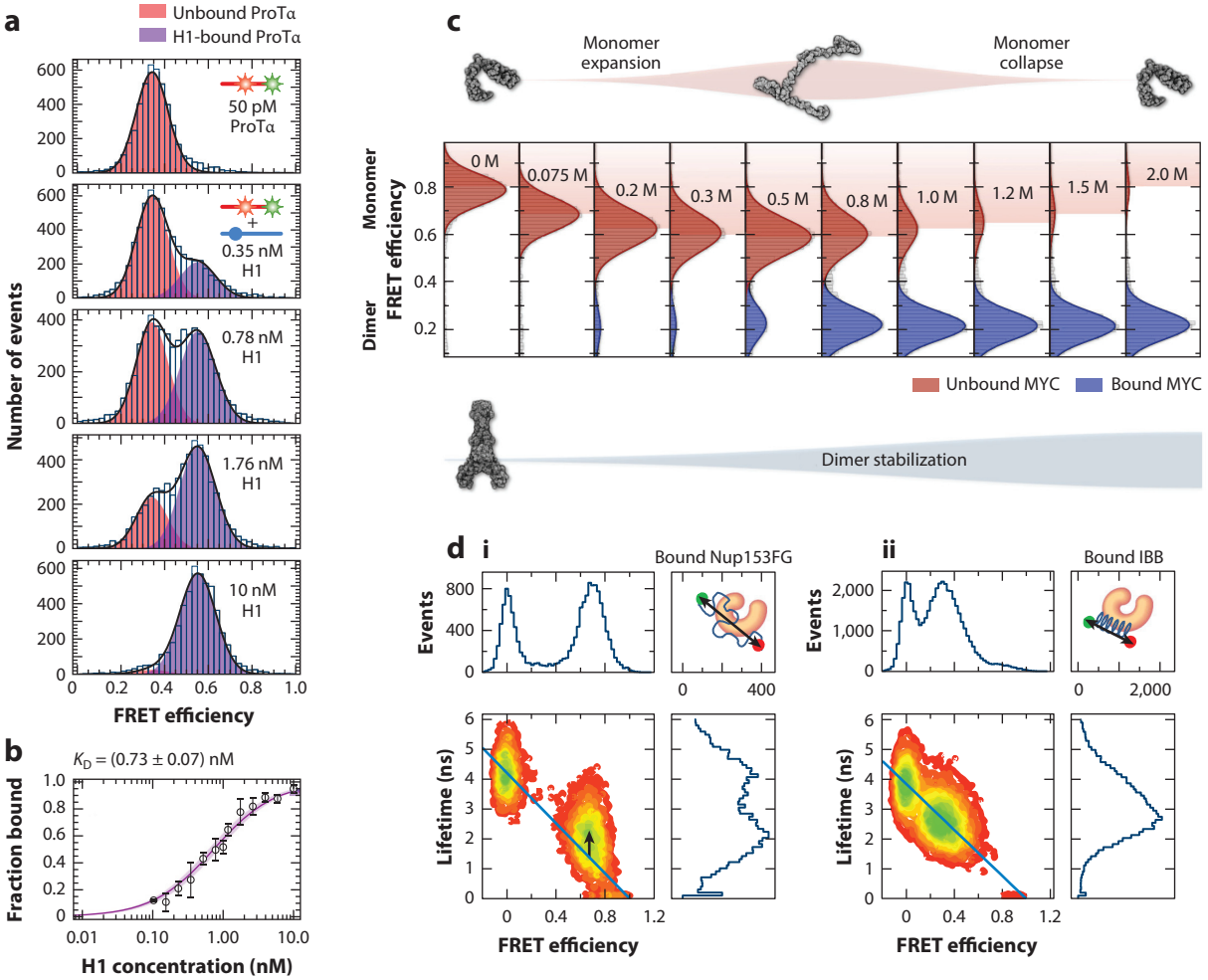

Figure 3

Probing IDP binding with single-molecule FRET. (*a*) Titration of doubly labeled ProTα with increasing concentrations of unlabeled H1, showing two peaks corresponding to unbound (*red*) and H1-bound (*purple*) ProTα (148). (*b*) Fraction of bound ProTα as a function of H1 concentration fitted with a binding isotherm (148). (*c*) Transfer efficiency histograms of doubly labeled MYC with a fixed concentration of unlabeled MAX at increasing KCl concentrations show two peaks corresponding to unbound (*red*) and bound (*blue*) MYC (163). Note the salt-dependent expansion and collapse of MYC (change in FRET efficiency) and the concomitant increase in MYC–MAX affinity (change in peak amplitudes). (*d*) Two-dimensional histograms of donor fluorescence lifetime versus transfer efficiency (see **Figure 2*c***) for Importin-β-bound IDPs, the FG domain of Nup153 (Nup153FG), and IBB. Nup153 retains disorder in the bound state, so the FRET population lies above the static FRET line (*i*), whereas for IBB, which folds upon binding, the population lies on the static line (*ii*) (27). Panels *a* and *b* adapted from Reference 148 (CC BY 4.0). Panel *c* adapted from Reference 163 (CC BY-NC-ND). Panel *d* adapted from Reference 27 (CC BY 4.0). Abbreviations: FRET, Förster resonance energy transfer; IBB, Importin-β-binding domain of Importin-α; IDP, intrinsically disordered protein.

motion of biomolecular complexes (**Figure 2*b***). FCS in free-diffusion experiments can be used for determining changes in translational diffusion coefficients—and thus hydrodynamic radii—upon binding (**Figure 2*e***), as well as for quantifying the concentrations of fluorescently labeled species (153, 181). Any of these observables can be employed for monitoring the interaction of an IDP with its target, provided that its change upon binding is sufficiently large.

A major benefit of single-molecule measurements compared to corresponding ensemble techniques is the spectroscopic separation of subpopulations (**Figures 2** and **3**). As a result, the relative populations of bound and unbound states and corresponding equilibrium constants can often be quantified directly from the integrated transfer efficiency peaks (**Figure 3*a*,*c***), and titrations covering a range of ligand concentrations can be analyzed with equilibrium models of binding (**Figure 3*b***). Spectroscopic observables can be extracted for individual subpopulations, and the response of their specific transfer efficiencies, stoichiometries, fluorescence lifetimes, anisotropies, etc., to solution conditions or temperature can be crucial for dissecting different contributions to affinity (148, 163), for instance, to identify the response of free and bound states to salt concentration (**Figure 3*c***). If the interconversion between bound and unbound states is fast relative to the observation time (approximately 1 ms in free-diffusion experiments), then only a single peak is observed that shifts continuously with ligand concentration. In this fast-exchange regime, the average signal, for example, the average transfer efficiency of the donor–acceptor-labeled population, can be employed to infer the fractional populations from the analysis of titrations with suitable binding isotherms.

This method enables affinities to be quantified across many orders of magnitude. Owing to the extreme sensitivity of single-molecule fluorescence, very high affinities with equilibrium dissociation constants, K_d, in the picomolar range have been measured (16, 60, 148). On the other extreme, since unlabeled ligands can be added at high concentrations, very low affinities with up to millimolar K_d have been quantified (45, 106). The separation of subpopulations enables complex binding equilibria to be dissected. Examples of such complex equilibria include the large number of conformational states that α-synuclein, a human IDP implicated in Parkinson's disease, exhibits in the presence of different concentrations of membrane-mimicking detergent and lipid vesicles (44, 159, 164), as well as the formation of ternary IDP complexes, which results in interesting allosteric effects (10, 11, 43, 60, 92, 148). The ability to work at very low protein concentrations confers an additional advantage, for example, for preventing aggregation or other nonspecific interactions (43).[3]

Employing multiparameter fluorescence spectroscopy is a powerful way of maximizing the available information and avoiding artefacts or the misinterpretation of data. For instance, if different observables yield different K_d values, then the binding mechanism may be more complex than a simple two-state process; very large fluorescence bursts in free-diffusion measurements are indicative of large aggregates or phase separation that may interfere with the measurement or need to be accounted for; changes in acceptor fluorescence lifetimes or molecular brightness upon binding may indicate quenching and cause a detection bias in the relative populations;[4] and large fluorescence anisotropies suggest a lack of rotational mobility of the dyes and indicate that caution is needed in the analysis of FRET efficiencies in terms of distances (61, 64, 86). Labeling positions should obviously be chosen in a way that minimizes interference with the binding process or other functions to be probed (179); the quantitative influence of fluorophore labeling on affinities can be assessed by employing different fluorophores and/or labeling positions (16, 17, 60, 167) or by comparing the affinities of labeled and unlabeled species, for example, in measurements where the labeled binding partner is outcompeted by the unlabeled binding partner (148).

[3]However, care needs to be taken to ensure that nonspecific adsorption of binding partners to the surface of the sample cell does not confound the results, for example, for highly positively charged IDPs (16).

[4]Note, however, that quenching or changes in fluorescence quantum yield in general can also be used as reporters of binding (39, 70).

ENSEMBLES AND DYNAMICS OF IDP COMPLEXES FROM SINGLE-MOLECULE FRET

Central to the behavior and binding mechanisms of IDPs are their structure and dynamics in the bound state. Especially in cases where substantial disorder is retained in the complex, single-molecule experiments can aid in the development of suitable models by providing information that is difficult to obtain with other methods. All of the observables mentioned above can be useful for this purpose, but—as in the case of unfolded and disordered proteins in isolation (67, 99, 107, 134)—intra- and intermolecular FRET efficiencies yield particularly valuable long-range distance constraints for mapping the heterogeneous conformational distributions of IDP complexes.

Ensembles of Disordered Complexes

A first important question that often needs to be addressed is whether structural disorder is present in the complex of interest. The broad and rapidly sampled distance distributions resulting from disorder can be identified in a combined analysis of fluorescence lifetimes and ratiometric transfer efficiencies (**Figure 2*c***). The deviation from the diagonal, the static FRET line, is related to the width of the underlying distance distribution (58, 73, 134).[5] The observed transfer efficiency then needs to be interpreted as an average over this distance distribution, rather than in terms of a single fixed distance (134). A reduction in the width of the distance distribution upon complex formation is a strong indication of folding upon binding (**Figures 2*c*** and **3*d***). Especially for highly disordered IDPs, analytical polymer models can provide useful approximations for their distance distributions (113, 134, 173, 178). IDP complexes comprising both disordered and folded elements may exceed the scope of such simple representations and often require more detailed molecular models or simulations (125, 140). Different strategies can then be employed (157) to obtain structural representations of IDP complexes. One is the use of experimental results, such as measured transfer efficiencies, directly as constraints in simulations, which is particularly useful if complete sampling of the distribution is difficult, i.e., in the case of large energetic barriers. Another strategy is to generate a prior conformational ensemble from unbiased simulations, which is then reweighted to obtain agreement with the experimental observables. It is noteworthy that, during the past decade, molecular dynamics force fields have made great progress toward faithfully representing the dimensions and dynamics of IDPs and thus often provide rather accurate prior ensembles, which may not even require reweighting (12). Finally, the parameterization of a simulation model—such as a coarse-grained representation—can be adjusted to optimize the agreement with the experimental data. A recent review (68) summarizes these methods in the context of single-molecule FRET on IDPs in general. In this section, we focus on examples where such methods have been used for IDP complexes.

One of the first cases where single-molecule FRET was utilized to elucidate an IDP complex ensemble was a study of the interaction of the IDP tau, which is implicated in Alzheimer's disease and modulates microtubule dynamics, with soluble tubulin heterodimers. Rhoades and coworkers (97) employed multisite single-molecule FRET and FRET-restrained coarse-grained modeling and observed that tau adopts a looped conformation facilitated by long-range

[5]Note that the variance of the observed transfer efficiency distribution itself, i.e., the width of the peak in the transfer efficiency histogram, is often dominated by shot noise, the statistical distribution of transfer efficiencies observed for individual molecules owing to the small number of photons per fluorescence burst (in a free-diffusion experiment) or per time bin (in a surface experiment). Only if the distance dynamics are slow enough (usually in the millisecond range or above) is a broadening of the transfer efficiency peaks beyond shot noise reliably detectable and employable for extracting information about the underlying distance distribution (if other sources of heterogeneity can be excluded) (1, 56, 110).

interactions between the termini (**Figure 4*a***). Tubulin binding impedes this interaction and favors an extended conformation of tau (95, 97, 108). Borgia et al. (16) used multisite intra- and intermolecular single-molecule FRET and multiparameter fluorescence analysis to probe the complex between two IDPs bearing large opposite net charges, linker histone H1.0 (H1, $z = +53$) and its nuclear chaperone, prothymosin α (ProTα, $z = -44$). Both proteins remain disordered and dynamic in the complex, although they interact with picomolar to nanomolar K_d in the physiological ionic strength range; a coarse-grained model with a single adjustable parameter (**Figure 4*b***) reproduced the 28 experimental transfer efficiencies and the distribution of chemical shift changes along the sequence (16). Similar electrostatically dominated interactions can drive the binding of IDPs to nucleic acids, as exemplified by the positively charged disordered nucleocapsid domain of the hepatitis C virus core protein bound to single-stranded nucleic acids (69) and H1 bound to nucleosomes (60). Also in these cases, coarse-grained simulations reproduced the experimental inter- and intramolecular transfer efficiencies (**Figure 4*d***). Both the nucleocapsid domain and the disordered regions of H1 remain disordered in the complex, and transient electrostatic interactions without site specificity are key determinants of such polyelectrolyte ensembles (60, 69, 132).

In another remarkable example, Wiggers et al. (167) showed that the disordered tail of the cell adhesion protein E-cadherin remains highly dynamic in complex with the folded protooncogene β-catenin; a coarse-grained model that reproduces the experimental transfer efficiencies illustrates how E-cadherin samples the surface of β-catenin diffusively without major free-energy barriers (**Figure 4*c***). Additional complexes in which IDPs retain their disorder in the bound state characterized by single-molecule FRET include FG-nucleoporin bound to nuclear transport receptor (101, 155); p27 bound to cyclin A/Cdk2 (161); the eukaryotic initiation factor 4E with its disordered binding proteins (143); and the apolipoprotein ApoE4, which was shown by a combination of single-molecule FRET and simulations to be much more disordered in its lipid-bound state than was previously thought (152). In general, we expect that multiple complementary biophysical methods, such as single-molecule FRET, NMR, SAXS, dynamic light scattering, EPR, neutron scattering and neutron spin echo spectroscopy (149), and molecular simulations, will increasingly be integrated to elucidate the conformational ensembles of IDP complexes (18, 132, 140).

Dynamics of Disordered Complexes

Understanding the behavior of IDP complexes requires not only a characterization of their equilibrium ensembles, but also the elucidation of their dynamics. Much of what we know about the conformational dynamics of IDPs and their complexes was discovered with NMR spectroscopy, which is ideally suited for probing aspects such as the rapid local motion in the pico- to nanosecond range and conformational exchange between subpopulations on the microsecond timescale and above (25, 40). One example of dynamics that have been difficult to assess quantitatively with NMR is the dynamics of global chain reconfiguration, i.e., the long-range conformational motion in disordered proteins. Single-molecule FRET spectroscopy is ideally suited to fill this gap, since it allows not only the average distance but also the distance fluctuations between donor and acceptor dyes to be quantified (109). The use of rapid fluorescence correlation methods has enabled the measurement of such distance dynamics down to the submicrosecond range, and this nanosecond fluorescence correlation spectroscopy (nsFCS) has thus increasingly been used to investigate the dynamics of IDPs (33, 101, 109, 131, 144, 167). The combination with nanophotonics now enables the resolution of even faster dynamics in the low nanosecond range (111).

Reconfiguration times of IDPs or their segments in the range of approximately 20 to 100 amino acids are commonly accessible in this way, which has typically yielded reconfiguration times of tens to hundreds of nanoseconds. The dynamics of most IDPs are slower than those of ideal polymers, which has been attributed primarily to intrachain interactions and dihedral barriers, resulting in

Reconfiguration time: the relaxation time of the distance correlation function between two residues in a (bio)polymer; characterizes long-range chain dynamics of IDPs

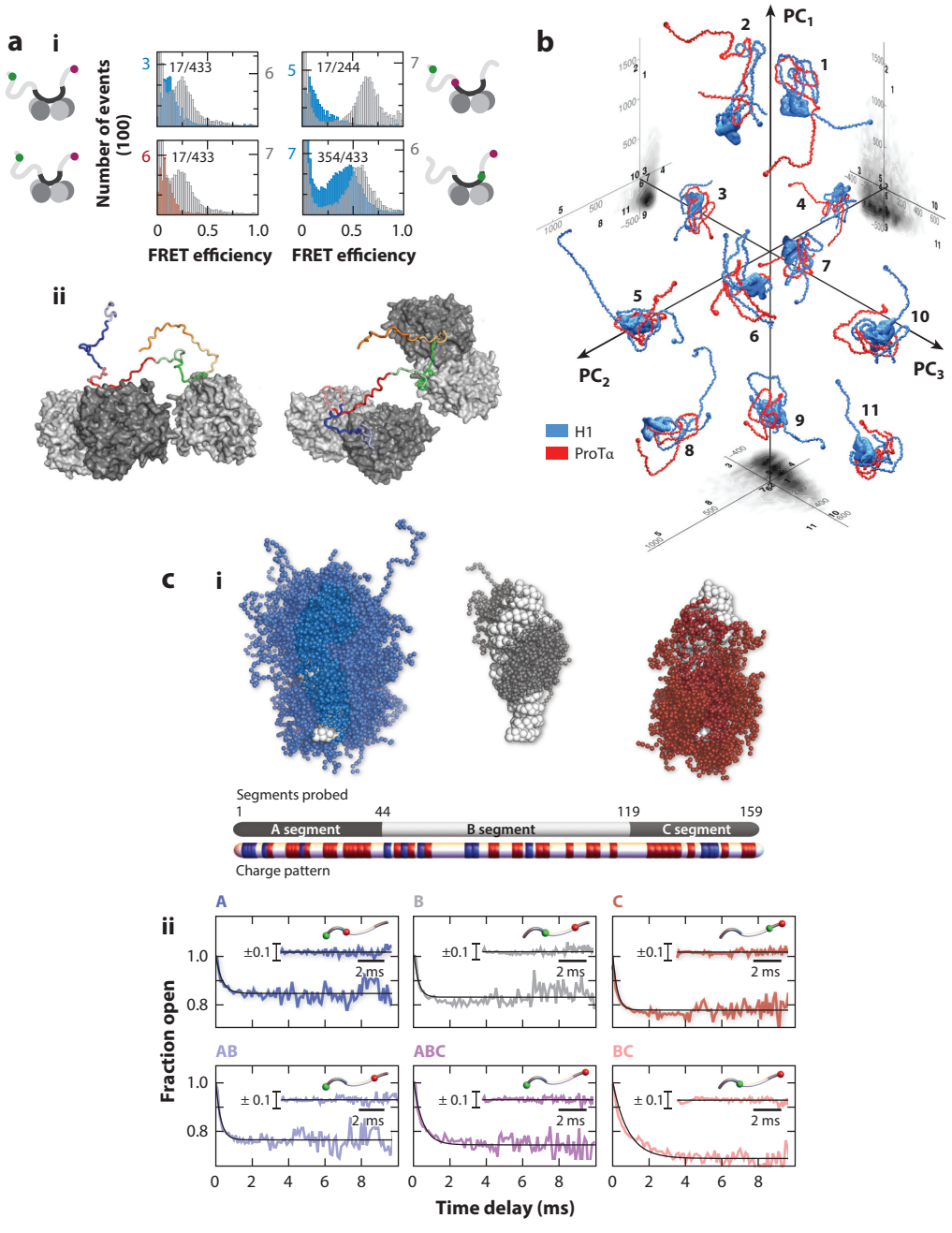

Figure 4

(*Continued*)

internal friction (4, 134, 145, 147, 172). Similar timescales have also been detected in several IDP complexes: The reconfiguration times probed with both intra- and intermolecular FRET in the electrostatically driven complexes of ProTα with H1 (16), the hepatitis C nucleocapsid domain with nucleic acids (69), H1 with the nucleosome (60) (**Figure 4*e***), and the reconfiguration time of nuclear transport factor–bound FG-Nups (101) are all between 10 and 200 ns. This behavior demonstrates that IDPs can retain their rapid chain dynamics even in high-affinity complexes if persistent local interactions are absent.

Internal friction: a solvent-independent dissipative force (friction) that slows down (bio)polymer dynamics

However, intra- and intermolecular interactions can slow down such dynamics substantially, as illustrated by the case of E-cadherin bound to β-catenin (**Figure 4*e***), which exhibits very broad transfer efficiency distributions, indicating slowly interconverting conformations, as has

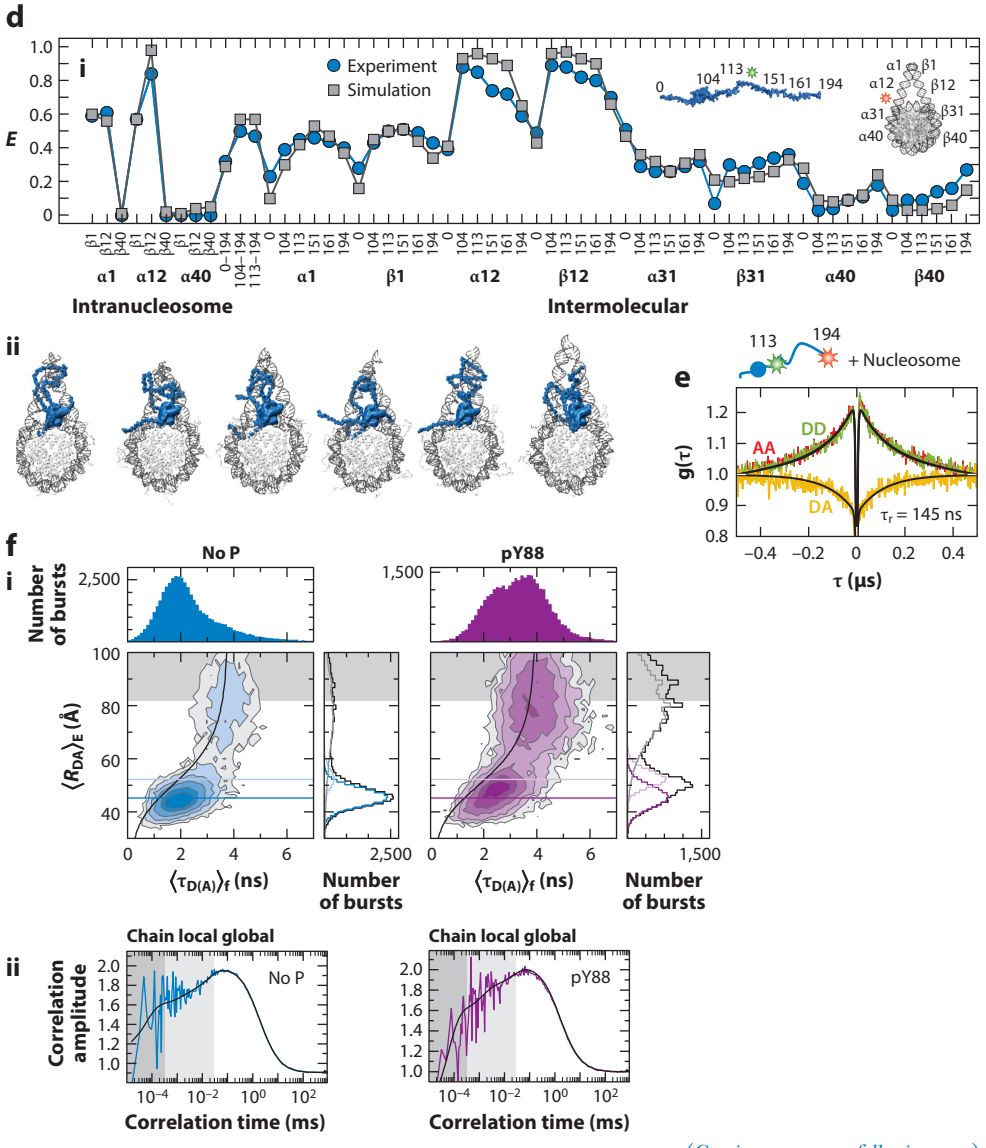

(*Caption appears on following page*)

Figure 4 (*Figure appears on preceding page*)

Ensembles and dynamics of disordered IDP complexes from single-molecule FRET–based modeling and simulations. (*a*) (*i*) Examples of transfer efficiency measurements of two isoforms of the IDP tau for different labeling sites, in the absence (*gray*) or presence (*blue* or *red*) of tubulin. (*ii*) Conformer of the microtubule-binding region of tau (*colored*) bound to tubulin (*gray*) from an ensemble of conformers generated via FRET-restrained Monte Carlo simulations, showing that the flexibility of tau allows for binding of multiple tubulin dimers (97). (*b*) Representative conformers of H1 (*blue*) and ProTα (*red*) in their highly disordered complex from coarse-grained simulations (16) (PC_1, PC_2, and PC_3 indicate the first three principal components of the distance map). (*c*) (*i*) Ensemble of the center-of-mass positions for different segments of the IDP E-cadherin (A in blue, B in dark gray, and C in red; see the schematic for sequence segments and charge patterning) bound to the folded β-catenin (*gray*) from a coarse-grained model informed by cystallographically resolved contacts and six measured transfer efficiencies (167). (*ii*) Recurrence analysis of the broad transfer efficiency histograms shows microsecond to millisecond dynamics of β-catenin on E-cadherin. (*d*) (*i*) Coarse-grained simulations (*gray*) reproduce the 57 transfer efficiencies, $\langle E \rangle$, measured in the H1–nucleosome complex (*blue*) (60) (for labeling positions, see annotated insets). (*ii*) Examples of conformers from the simulations, with the globular domain of H1 bound at the nucleosome dyad axis and the C-terminal region remaining disordered (60). (*e*) nsFCS of double-labeled H1 on the nucleosome: Donor (*green*) and acceptor (*red*) autocorrelations and donor–acceptor cross-correlation (*gold*) yield a reconfiguration time of 145 ns, reflecting rapid long-range dynamics of H1 in the bound state (60). (*f*) Dimensions and dynamics of cyclin A/Cdk2-bound p27. (*i*) Two-dimensional histograms of the FRET-averaged donor–acceptor distance versus donor fluorescence lifetime and the corresponding one-dimensional projections for unphosphorylated and Y88-phosphorylated p27. The gray-shaded area indicates molecules without an active acceptor, and the black line represents the static FRET line (161). (*ii*) Cross-correlation functions from filtered correlation analysis for p27 in complex with cyclin A/Cdk2 without (*left*) and with (*right*) phosphorylation (161). Panel *a* adapted from Reference 97. Panel *b* adapted from Reference 16. Panel *c* adapted from Reference 167 (CC BY). Panels *d* and *e* adapted from Reference 60. Panel *f* adapted from Reference 161 (CC-BY). Abbreviations: FRET, Förster resonance energy transfer; IDP, intrinsically disordered protein; nsFCS, nanosecond fluorescence correlation spectroscopy.

been confirmed by the dynamics in the range of hundreds of microseconds observed in recurrence analysis (167). These conformations are not separated by well-defined free-energy barriers; instead, a rugged free-energy surface causes slow diffusive sampling of the β-catenin surface by E-cadherin. A broad range of dynamics from approximately 60 ns to 250 μs was observed for the disordered cell-cycle regulator p27 bound to the cyclin A/Cdk2 complex (161) based on multiparameter correlation analysis of subpopulations (15, 42) (**Figure 4*f***). These dynamics reflect a complex free-energy surface, and the intrinsic flexibility of p27 is essential for kinase activation by phosphorylation. The number of systems that have been investigated in such detail is still quite limited, so broader coverage will be essential for a full view of the rich timescales and types of dynamics involved in IDP complexes.

FROM COUPLED FOLDING AND BINDING TO BINDING DECOUPLED FROM FOLDING—BEYOND SIMPLE MECHANISMS

The abundance of IDPs in cellular interaction networks raises the question of whether—and if so, how—their binding mechanisms and kinetics differ from the well-established paradigms of fully folded proteins (129). This and related questions have increasingly been addressed experimentally, including the role of electrostatics, the mechanisms of coupled folding and binding, and allosteric effects (10, 11, 43, 52, 60, 92, 138, 148). How can single-molecule experiments, with their potential for resolving structural and kinetic heterogeneity, contribute to interrogating kinetic mechanisms?

Nonequilibrium Kinetics

In analogy to the typical perturbation methods employed for ensemble experiments, nonequilibrium kinetics of single molecules can be probed by manual or—if the process is faster than about a

minute—by rapid microfluidic mixing. Microfluidic devices are particularly suitable for the combination with confocal detection because of their geometry, and they have the additional advantage of very low sample consumption (93, 120, 170). Dead times in the millisecond range (120) and even below (50) can be achieved by hydrodynamic focusing (82), and long observation channels can extend the observation times to a few minutes (170) to enable overlap with the shortest times accessible by manual mixing (9). Recording single molecules at different points along the observation channel yields the signal at different times after mixing, such as the relative populations of free and bound protein.

Encounter complex: a loosely bound transient state formed during binding, largely stabilized by nonspecific interactions between the binding partners

Gambin et al. (50) used such devices to investigate the SDS-induced folding of α-synuclein and observed the very rapid formation of transient structures in the binding of α-synuclein to SDS that they identified as encounter complexes. Recent developments in single-molecule microfluidics include a double-jump mixing device, which combines two consecutive rapid mixing steps separated by an intermediate delay channel (38). The device allows transient intermediates to be populated and has been employed to measure the association and dissociation kinetics of the coupled folding and binding of the IDPs ACTR and NCBD in a single experiment. The limitation that intermolecular single-molecule FRET experiments are only possible at very low sample concentrations (and thus very high affinities) has recently been removed by microfluidic rapid dilution devices, which allow a concentrated sample to be diluted by up to five orders of magnitude within milliseconds (62, 176) (**Figure 5*a***). By preforming IDP complexes at high concentrations and then diluting them rapidly to single-molecule concentrations, one can interrogate even interactions with affinities in the micromolar range with intermolecular two- and three-color FRET before and during dissociation (176). Microfluidic devices have thus become an important part of the single-molecule tool kit for probing IDP interactions.

Equilibrium Kinetics

A remarkable aspect of single-molecule experiments is that kinetics can be investigated at equilibrium, without requiring a perturbation, provided that the interconversion between the states of interest occurs frequently enough at equilibrium to yield adequate statistics during the available observation time. To enable sufficiently long recordings, such measurements are most commonly performed by immobilizing one binding partner on a surface[6] and having the other binding partner(s) free in solution. There are two popular ways of monitoring binding and dissociation via FRET. In the intramolecular approach, the surface-immobilized molecule is labeled with donor and acceptor, and the binding partner in solution is unlabeled. This method requires a conformational change in the surface-immobilized molecule upon binding that yields a sufficiently large change in FRET efficiency (or another spectroscopic signal), but it has the advantage that the unlabeled molecule in solution can be added at high concentration, so that even low-affinity interactions can be probed (45). The alternative approach is an intermolecular FRET experiment, where the surface-immobilized molecule is donor-labeled, and the molecule in solution is acceptor-labeled.[7] In this case, binding can lead to a very large change in transfer efficiency and provide excellent contrast between bound and unbound states (180), but the fluorescence background from the labeled molecules in solution usually limits accessible concentrations to the low

[6]To minimize nonspecific interactions with the surface, suitable coating of the surfaces is usually required, most frequently with polyethylene glycol (PEG) brushes, doped with biotinylated PEG to enable immobilization of biomolecules via biotin–avidin coupling.

[7]It is of course also possible to surface-immobilize the acceptor-labeled molecules and have the donor-labeled partner free in solution, but the higher fluorescence background from the molecules in solution upon donor excitation limits the concentration range that can be used more than in the other permutation.

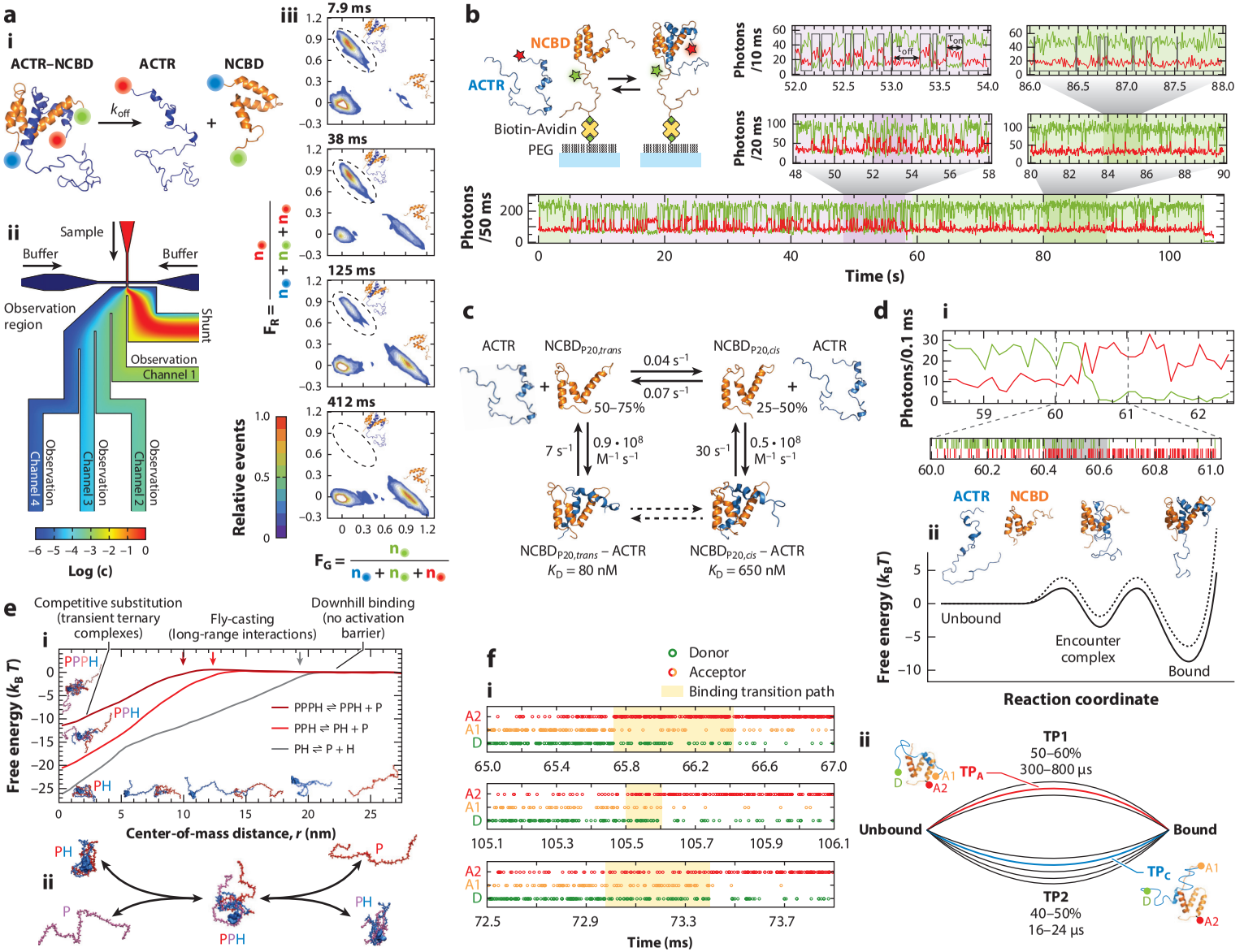

(Caption appears on following page)

Figure 5 (*Figure appears on preceding page*)

Kinetics of IDP interactions probed by single-molecule FRET. (*a*) Dissociation kinetics of low-affinity complexes probed by three-color FRET and rapid microfluidic dilution of the ACTR–NCBD complex (see cartoon, *i*). (*ii*) Device layout and concentration profile during dilution (see color scale) (176). (*iii*) Two-dimensional histograms of three-color photon count ratios measured after rapid dilution enable FRET efficiencies and populations to be monitored as a function of time (see legends). (*b*) Detecting kinetic heterogeneity caused by peptidyl-prolyl *cis/trans* isomerization in measurements of surface-immobilized NCBD binding to ACTR (see cartoon). The single-molecule trajectory shows donor (*green*) and acceptor fluorescence (*red*), with progressive magnifications of segments revealing longer- (*pink shading*) and shorter-lived (*light green shading*) complexes (180). (*c*) Resulting four-state kinetic scheme of ACTR–NCBD complexation with rate coefficients that differ for the two relevant peptidyl-prolyl isomers in NCBD (180). (*d*) Transition-path measurements of coupled folding and binding. (*i*) Fluorescence time trace with a single ACTR–NCBD binding event observed by intermolecular FRET (see cartoon in panel *a*), time-binned and as single-photon data (gray shading indicates the transition-path region) (153). (*ii*) Schematic of the resulting free-energy surface of NCBD–ACTR complexation at different salt concentrations with high-energy encounter complex (see cartoons) (153). (*e*) (*i*) Potentials of mean force for H1–ProTα binding (H indicates H1; P indicates ProTα) from coarse-grained simulations illustrate key kinetic and dynamic aspects of disordered complexes (148), as annotated, including the formation of transient trimers and tetramers (in this case for excess P). (*ii*) Kinetic scheme of competitive substitution via transient ternary complex (PPH) formation (148). (*f*) Characterization of transition-path heterogeneity in coupled folding and binding for NCBD and TAD using three-color FRET. (*i*) Representative three-color photon time traces (green circles indicate donor photons; orange and red indicate photons from acceptors) near the binding transition path (*yellow shading*) (78). (*ii*) Schematic with the two classes of transition paths with different durations. Panel *a* adapted from Reference 176 with permission from John Wiley & Sons. Panels *b* and *c* adapted from Reference 180 (CC BY). Panel *d* adapted from Reference 153 (CC BY). Panel *e* adapted from Reference 148 (CC BY). Panel *f* adapted from Reference 78 with permission from The American Association for the Advancement of Science. Abbreviations: FRET, Förster resonance energy transfer; IDP, intrinsically disordered protein.

nanomolar range or below. As a consequence, only high-affinity interactions can be probed in this way.

One of the first studies that took advantage of single-molecule FRET for monitoring conformational fluctuations and binding of an IDP investigated the marginally stable transcriptional regulator IκBα, which exhibits spontaneous local unfolding under native conditions but can be stabilized by binding to NFκB (87). To quantify the conformational fluctuations involved, the authors used the cross-correlation of donor and acceptor signal, which is a very useful and generally applicable approach for assessing the timescales of even complex distance fluctuations in a model-free manner. The authors observed dynamics on the timescale of approximately 1 s and below, but the frame rate of the camera limited the time resolution to 100 ms. Faster kinetics down to approximately 1 ms can be observed with more recently available scientific CMOS cameras (72) or with confocal detection using avalanche photodiodes for single-photon counting with time resolution in the picosecond range (limited by the timing jitter of detection; see examples below). The kinetic information in single-molecule time traces is essentially contained in the dwell-time distributions of the different states and their connectivity (126). State-of-the-art analysis methods typically combine hidden Markov models with likelihood maximization (57, 96), and promising nonparametric Bayesian methods to address issues such as the model selection bias are currently under development (65, 137).

Resolving Complex Kinetics

The opportunity to monitor a broad range of timescales in single-molecule time traces enables the detection of even complex kinetics, of which several examples have recently been reported in the context of IDP interactions. One case involves the effect of peptidyl-prolyl *cis/trans* isomerization, a process that occurs on the timescale of seconds to minutes (80). Zosel et al. (180) used confocal single-molecule FRET to monitor the influence of peptidyl-prolyl *cis/trans* isomerization on the interaction kinetics between ACTR and NCBD, a classic example of coupled folding and binding (36). They identified a conserved proline residue in NCBD whose *cis/trans* isomerization modulates the association and dissociation rates with ACTR. As a result, NCBD switches on a

timescale of tens of seconds between two populations that differ in their affinities to ACTR by approximately an order of magnitude (**Figure 5*c***). The beauty of single-molecule trajectories is that kinetic heterogeneity can be apparent even by visual inspection (**Figure 5*b***). Since proline is highly enriched in IDPs compared to folded proteins (156), it is likely to have a widespread influence on IDP binding processes (46, 54). Another case is the interaction of the hepatitis C virus core protein with nucleic acids, where the kinetic heterogeneity originating from coupled folding and binding was detected in single-molecule trajectories. Holmstrom et al. (69) found that this positively charged viral IDP remains disordered upon binding but facilitates the formation of DNA and RNA structure. By acting as a flexible macromolecular counterion, the protein locally screens repulsive electrostatic interactions with an efficiency equivalent to molar salt concentrations. The change in DNA or RNA folding kinetics and stability upon IDP binding was apparent from the measured time traces, and the underlying mechanism could be rationalized by simulations.

Ternary complex: three molecules bound to each other; ternary complexes can lead to complex allosteric and kinetic effects

Competitive substitution: rapid exchange of binding partners via a short-lived ternary complex of interacting (bio)polymers

The complexity of interaction mechanisms can be increased further by the formation of higher-order complexes (ternary, quaternary, etc.), in which more than two biomolecules interact simultaneously. In general, higher-order complex formation is facilitated by multivalency, and it has most often been reported for DNA binding, where it can lead to concentration-enhanced dissociation (11, 26). The interactions of highly charged IDPs that remain disordered in the bound state (132) can be considered an extreme case of multivalency: Since no persistent residue-specific interactions are formed, they are particularly conducive to the formation of higher-order complexes, and unexpected concentration-dependent interaction mechanisms can emerge.

This behavior is illustrated by the example of the complex between the highly positively charged histone H1 and the highly negatively charged ProTα. At protein concentrations in the picomolar and low nanomolar range, both the equilibria (16) and kinetics (148) of the interaction between these two biological polyelectrolytes are well described by a simple two-state binding mechanism with 1:1 stoichiometry: The observed association rates increase linearly with the concentration of binding partner, and the dissociation rate constants exhibit the characteristic concentration independence. However, as the protein concentrations are increased to the micromolar range, the interconversion between bound and unbound states becomes much faster than expected from simple two-state binding, resulting in exchange behavior that is rapid on the millisecond timescale both in single-molecule and in NMR measurements (148). This switch in kinetic mechanism can be explained by the formation of ternary complexes: The disorder of H1 and ProTα in the 1:1 complex facilitates the association of an additional copy of H1 or ProTα with micromolar affinity (**Figure 5*e***). The low affinity favors rapid dissociation of one of the protein molecules that are present twice in the complex, and since the submicrosecond reconfiguration times in the complex ensure rapid randomization of all interchain configurations, each molecule has a 50% chance of dissociating. The result of this competitive substitution (118) via a short-lived ternary complex is a rapid exchange of binding partners (148).

Molecular simulations rationalize several key properties of this interaction mechanism (**Figure 5*e***). First, they confirm the feasibility of ternary complex formation with reduced affinity compared to the binary complex and the resulting competitive substitution. Simulations also illustrate the possibility of forming higher-order complexes, in agreement with experiment (16, 148). Second, the potential of mean force obtained from umbrella sampling is devoid of an activation barrier. The corresponding downhill binding explains the diffusion-limited association rates obtained experimentally for IDPs forming disordered complexes (60, 101). Finally, simulations show an interaction between the proteins at distances much greater than their added radii of gyration. This fly-casting mechanism (141) further accelerates association. Altogether, such charged disordered complexes thus enable both rapid association and rapid dissociation despite their very high affinities.

The importance of these interaction mechanisms for biological function is illustrated by the effect of ProTα on the binding of the linker histone H1 to the nucleosome (60). H1 binds to nucleosomes near the entry and exit regions of the linker DNA that connects different nucleosomes (**Figure 4*d***), which leads to nucleosome compaction and, on a larger scale, to chromatin condensation (63). However, the H1–nucleosome affinity at physiological salt concentrations in vitro is in the femtomolar range (60), corresponding to very slow spontaneous dissociation of H1, incompatible with rapid transcriptional regulation in the cell. Single-molecule kinetics and molecular simulations show that ProTα, which has previously been shown to act as a linker histone chaperone in cells (51), competes for binding to H1 and accelerates H1 dissociation by invading the H1–nucleosome complex, screening the charge interactions of H1 with the nucleosomal DNA, and dissociating with H1 (60). Ternary complex formation of highly charged disordered protein complexes and the resulting competitive substitution can thus explain the histone-chaperoning mechanism of ProTα. In view of the abundance of highly charged nucleic acids and IDPs in the nucleus (13, 48), similar interactions and mechanisms may be prevalent in chromatin and many of the pertinent regulation processes. In summary, the quantitative analysis of single-molecule kinetics can thus be a valuable approach for understanding interaction mechanisms.

Transition path: the short part of a reaction during which the free-energy barrier between reactants and products is crossed

Transition Paths

Not only can single-molecule spectroscopy reveal kinetics in terms of reaction rates, which are related to the waiting times in the minima of the underlying free-energy surfaces, but it can also resolve the actual barrier crossing processes, the transition paths, which contain most of the mechanistic information (28, 66). First steps in leveraging this approach for the interaction mechanisms of IDPs have recently been taken (**Figure 5*d***). Kim et al. (79) and Sturzenegger et al. (153) investigated the coupled folding and binding of NCBD with the transactivation domain (TAD) of the tumor suppressor protein p53 and with ACTR, respectively. In both cases, transition path times in the range of approximately 100 μs at near-physiological salt concentrations were observed, surprisingly long compared to the association between the folded proteins barnase and barstar (79) or the folding of a monomeric protein (28). The cause of this disparity is the formation of an encounter complex (or transient complex), an intermediate in which the two proteins have already bound to each other but have not yet formed a stable folded structure.

However, the transition paths of binding for TAD and ACTR to NCBD also exhibit interesting differences. For instance, although the association rate constants showed a pronounced increase with decreasing salt concentration in both cases, the lifetimes of the encounter complexes behave differently: For TAD–NCBD, the lifetimes increase at low salt concentration (79), whereas the lifetime for ACTR–NCBD is virtually independent of salt (153), indicating different roles of Coulomb interactions in the encounter complexes of the two protein pairs. For ACTR–NCBD, both the viscosity dependence and the distribution of the transition path times largely exclude internal friction or roughness of the free energy surface as major contributions to complex formation (153). An aspect that complicates the analysis of processes such as coupled folding and binding of IDPs is the potential heterogeneity of microscopic pathways, in analogy to protein folding (41). Kim & Chung (78) recently combined the analysis of transition path times with three-color FRET experiments to address this challenging question for TAD–NCBD. They concluded that approximately half of the transitions follow a slow path with transition times of several hundred microseconds involving strong electrostatic interactions between the C-terminal region of TAD and NCBD, and the other half takes binding paths that are an order of magnitude shorter, characterized by more prevalent interactions of the middle region of TAD with NCBD (**Figure 5*f***). Technically advanced approaches of this type may allow us to resolve ever more mechanistic details of IDP interactions.

Oligomers, Aggregates, and Biomolecular Condensates

Liquid–liquid phase separation: spontaneous demixing of a homogeneous liquid into two mesoscopically distinct phases (for biomolecular solutions usually a dilute and a concentrated phase)

Macromolecular crowding: the influence of mutual volume exclusion on macromolecules within a crowded medium, including effects on their conformations and interactions

An important challenge is to take our investigations beyond small oligomers, since IDPs are often involved in supramolecular association, such as amyloidogenesis or liquid–liquid phase separation (LLPS). Amyloid-associated pathologies such as Parkinson's disease, Alzheimer's disease, and amyotrophic lateral sclerosis involve aberrant aggregation of IDPs, such as tau, α-synuclein, FUS, TDP-43, or hnRNPA1 (171). Formation of amyloid fibrils often occurs via complex kinetic pathways involving oligomeric species, which may themselves contribute to disease pathology (22). Klenerman, Dobson, and coworkers used unlabeled IDPs doped with picomolar concentrations of donor-labeled and acceptor-labeled molecules, which afforded single-molecule fluorescence detection. They reported distinct oligomeric intermediates, their sizes, concentrations, and conformational classes (116), and they identified a slow structural transition of oligomers preceding fibril formation (32, 71, 139). α-Synuclein oligomers after the structural transition were more cytotoxic to neurons than were early oligomers (32). A similar strategy was used to identify oligomers of other IDPs, for example, for FG-Nups during osmolyte-induced fibrillation (100). High-resolution imaging approaches can be used to complement single-molecule experiments (98, 122).

Although these approaches afford information about aggregation mechanisms and kinetics, they provide little conformational detail. In an alternative approach, Chung and coworkers (30) used elegant two- and three-color FRET experiments combined with fluorescence lifetime analysis to dissect the oligomerization of the disordered tetramerization domain of p53 (**Figure 6*a***). Although the kinetics are very slow (124), and the dissociation constants of dimer and tetramer are very similar, the authors succeeded in quantifying the kinetic rate coefficients for dimerization and tetramerization and probed the associated structural changes from the disordered monomer to the folded oligomers (30). Stoichiometrically less well defined oligomerization has been observed for ProTα–H1 complexation: Adding a large excess of ProTα or H1 causes a continuous shift in transfer efficiency and hydrodynamic radius, indicating the progressive formation of larger and larger oligomers (16, 148), as supported by simulations (**Figure 5*e***).

LLPS involving IDPs has been heavily investigated in the past decade (20, 37), but it has remained relatively unexplored with single-molecule methods, probably at least in part owing to technical challenges such as autofluorescence in the protein-dense condensates. The interactions that encode the dimensions of IDPs resemble those that lead to phase separation (20, 21, 37, 94); considering the progress facilitated by single-molecule FRET in deciphering the polymer physics of IDPs per se (134), its application to LLPS will be an important next step (99, 107). Particularly interesting aspects to be addressed with this approach are the conformational distributions and dynamics of IDPs within condensates (19, 24), a largely uncharted territory where single-molecule FRET can make inroads (102, 103). A recent investigation of tau with single-molecule FRET indicated an expansion in the dense compared to the dilute phase (**Figure 6*b***), which may be important for promoting intermolecular association and fibrillation (166), similar to other cases where LLPS and aggregation have been suggested to be linked (171). As in amyloid formation, oligomers may also be important as intermediates in LLPS (76, 135, 166).

Toward Cellular IDP Interaction Dynamics

Ultimately, we seek to understand IDP interactions quantitatively inside the cell (123). An important advantage of single-molecule spectroscopy in this context is the ability to observe specifically labeled biomolecules even in complex environments. A first step is to mimic individual cellular effects in vitro, such as macromolecular crowding or posttranslational modifications (PTMs). The volume fraction of biological macromolecules in the cell is approximately 10–40% (14, 177), and

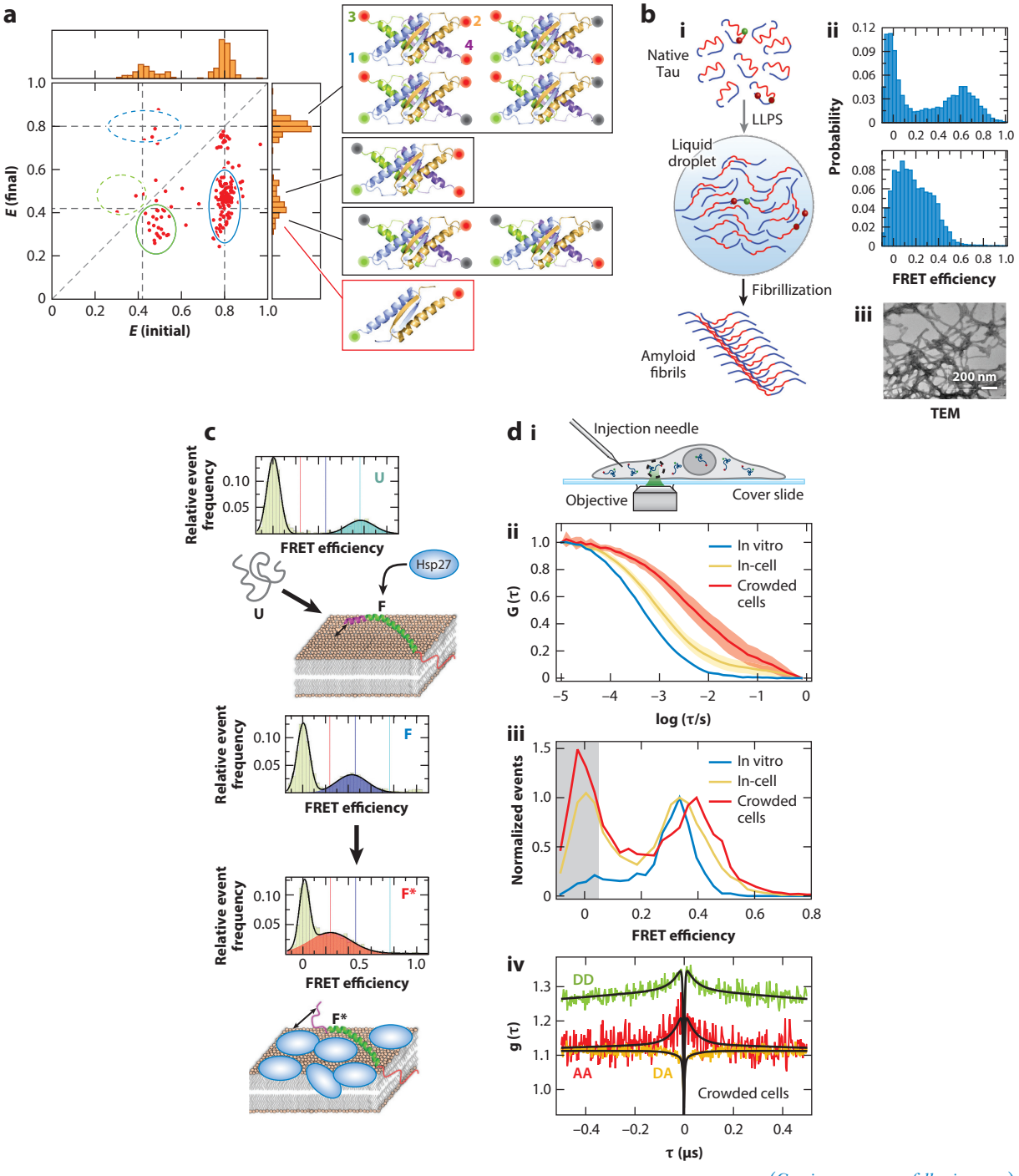

(Caption appears on following page)

Figure 6 (*Figure appears on preceding page*)

IDP oligomerization, phase separation, and in-cell behavior. (*a*) Tetramerization of the p53 tetramerization domain probed with single-molecule FRET (30). Transition maps from transfer efficiencies before [FRET efficiency (initial)] and after [FRET efficiency (final)] transitions are observed with immobilized donor-labeled p53 in the presence of acceptor-labeled p53-Tet, with the expected efficiencies of the different species. (*b*) Single-molecule FRET of phase separation. (*i*) Schematic of tau fibrillation via LLPS. (*ii*) Transfer efficiency histograms of tau in dilute solution and in phase-separated droplets indicate expansion of tau in droplets, which might facilitate fibrillation (*iii*: electron micrograph of fibrils) (166). (*c*) Effect of 2D crowding on α-synuclein. Transfer efficiency histograms are shown of α-synuclein in solution (*cyan*), membrane-bound (*blue*), and membrane-bound in the presence of HSP27 acting as a 2D crowder (*red*) (8), with a cartoon illustrating the different conformations. (*d*) In-cell single-molecule spectroscopy. From top to bottom are shown a cartoon of microinjection of labeled molecules into an adherent eukaryotic cell and subsequent confocal single-molecule measurement (84); FCS of labeled ProTα in buffer solution, in untreated cells, and in cells under hyperosmotic shock (crowded cells), showing increased retardation of translational diffusion (83); corresponding transfer efficiency histograms of labeled ProTα showing an increase in transfer efficiency in crowded cells, corresponding to chain compaction (83); and nsFCS of labeled ProTα in crowded cells with donor–donor (*green*), acceptor–acceptor (*red*), and donor–acceptor correlation showing fast nanosecond reconfiguration times (83). Panel *a* adapted from Reference 30. Panel *b* adapted from Reference 166 (CC BY-NC-ND). Panel *c* adapted from Reference 8 with permission from John Wiley & Sons. Panel *d* adapted from References 83, with permission from John Wiley & Sons, and from Reference 84. Abbreviations: FCS, fluorescence correlation spectroscopy; FRET, Förster resonance energy transfer; IDP, intrinsically disordered protein; LLPS, liquid–liquid phase separation; nsFCS, nanosecond FCS; TEM, transmission electron microscopy.

their entropic volume exclusion can affect biomolecular conformations and interactions (74, 174). Indeed, using single-molecule FRET, Soranno et al. (146) observed a compaction of IDPs not only with increasing concentration but also with increasing size of the crowding agents, at variance with the predictions from scaled-particle theory (53), the prevalent paradigm in the field. However, this behavior can be explained quantitatively if the polymeric nature of both the IDPs and the crowders is explicitly taken into account (146). Zosel et al. (181) addressed the effect of crowding on IDP interactions, specifically the binding of ACTR to NCBD. Single-molecule spectroscopy allowed them to quantify the effects of crowding on several key observables simultaneously: the equilibrium stability of the complex from free-diffusion or surface experiments, association and dissociation kinetics from time traces of immobilized molecules, and the microviscosity governing translational diffusion from FCS. A quantitative explanation of the stabilization of the complex, the crowder size dependence of diffusivity, and the nontrivial effects on kinetics was possible within the framework of depletion interactions, but only if the polymeric nature of IDPs and crowders was accounted for (181). Interesting crowding effects have also been observed for α-synuclein interacting with a lipid bilayer (8) (**Figure 6*c***). α-Synuclein undergoes a transition to extended helical conformers upon membrane binding, and the additional binding of Hsp27 to the lipid bilayer induces an otherwise absent conformer of α-synuclein via a bimodal inhibition mechanism.

In vivo, IDPs are subject to extensive PTMs, which can modulate their dimensions, dynamics, interactions, and other functions (6, 121). For FG-Nups, glycosylation was shown by single-molecule FRET to result in chain expansion, but it had no effect on their recognition by nuclear transport receptors (155). For disordered p27 bound to the cyclin A/Cdk2 complex, single-molecule FRET revealed two dynamic conformers (**Figure 4*f***), corresponding to tightly and loosely bound p27, that exchange on a millisecond timescale. Interestingly, these two populations are present irrespective of p27 phosphorylation, but site-specific phosphorylation increases the fraction of the loosely bound conformer, which is likely to constitute the molecular basis of signal transduction by p27 (161). Owing to the biochemical challenges in obtaining site-specifically phosphorylated IDP samples, phosphomimetic amino acid substitutions have been used for probing binding and folding of the disordered N terminus of nucleophosmin by single-molecule FRET (7). In summary, a strength of single-molecule spectroscopy is that it resolves conformational and kinetic heterogeneity, which is expected to be caused by nonuniform modifications in vitro and especially in vivo. Interesting next steps may involve mimicking more realistic cellular conditions,

for example, by using cell lysates or reconstituted cytoplasm (128). Eventually, however, a key goal will be to monitor IDPs and their interactions directly in live cells, and recent advances in in-cell single-molecule methods (84, 123, 127, 146, 150) provide promising tools for such measurements.

In-cell single-molecule spectroscopy has primarily been impeded by the technical challenges associated with cellular autofluorescence and with obtaining the required well-controlled concentrations of site-specifically labeled fluorescent molecules inside cells. Background problems are mitigated by working at wavelengths >520 nm, where cellular autofluorescence drops off (3). Since fluorescent proteins are suboptimal for quantitative single-molecule FRET spectroscopy, dye-labeled proteins need to be introduced into cells. Several strategies have been used, such as microinjection into mammalian cells (83, 84, 127) (**Figure *6d***), electroporation into bacterial cells (31), fast labeling chemistries combined with tightly controlled expression (2), and nonsense codon suppression with transfer RNAs acylated with fluorophore-labeled amino acids (90). Each of these strategies has its strengths and weaknesses. Microinjection of fluorescently labeled proteins, for example, transiently perturbs the cell, but it yields rather reproducible intracellular concentrations, allows injections selectively into the nucleus or the cytoplasm, and offers great flexibility in terms of the choice of proteins. Using this strategy, König et al. (84) investigated ProTα in adherent eukaryotic cells using single-molecule FRET and nsFCS and found its dimensions and chain dynamics to be very similar to those in buffer, suggesting minimal intracellular interactions and crowding effects. However, a reduction in cell volume by only a factor of two caused by hyperosmotic stress leads to a significant collapse of ProTα, slowed chain dynamics, and much slower translational diffusion (**Figure *6d***), indicating that crowding effects are highly dependent on the macromolecular concentration and on the length scale probed (83). Although such studies are only initial steps toward the routine application of single-molecule spectroscopy in live cells, they demonstrate that exciting insights can be gained. Examples of promising current developments for further expanding the scope of single-molecule experiments in cells are the MINFLUX technique (59), the combination of amber codon suppression with photoactivable FRET dyes (119) to enable the precise tuning of concentrations akin to the procedures used in photoactivable localization microscopy (PALM) (117), and the direct combination of superresolution techniques with FRET (23, 154).

SUMMARY POINTS

1. A broad spectrum of structural disorder is present in complexes formed by IDPs, and single-molecule spectroscopy provides a versatile and growing tool kit for its investigation. Important experimental observables include transfer efficiency (reporting on intra- or intermolecular distances), stoichiometry, fluorescence anisotropy (reporting on rotation and local dynamics), fluorescence lifetime (reporting on conformational distributions), and fluorescence correlations (reporting on a wide range of dynamics).
2. Timescales from nanoseconds to hours, from chain reconfiguration to translational diffusion and kinetics of binding or aggregation, can be probed via single-molecule spectroscopy in both nonequilibrium and equilibrium measurements.
3. IDPs in their complexes can remain highly disordered and dynamic, and long-range chain reconfiguration times between approximately 100 ns and 1 ms have been observed. These timescales are likely to be governed by the absence or presence of persistent local interactions resulting in internal friction or energetic roughness.

4. Disordered complexes can give rise to a wealth of interaction mechanisms beyond simple two-state binding. Examples include fly-casting; disorder-mediated encounter complexes; competitive substitution via ternary complexes; and the formation of large oligomers, assemblies, and aggregates.
5. The specific roles of IDP complexes for biological function are beginning to emerge, including their impact on allostery, the rapid dissociation of even high-affinity complexes by competitive substitution, their pronounced accessibility to PTMs, and their sensitivity to macromolecular crowding and the cellular environment.

FUTURE ISSUES

1. The examples of disordered complexes observed to date are likely to be just the tip of the iceberg, and the developments in single-molecule spectroscopy present a great opportunity for elucidating interesting dynamics and previously unidentified interaction mechanisms.
2. Integration of single-molecule spectroscopy with other biophysical experiments, theory, and simulations will enable further advances in elucidating the molecular properties and functions of IDP complexes.
3. There is likely to be an entire spectrum of IDP oligomerization, ranging from simple one-to-one complexes all the way to phase separation and aggregate or amyloid formation. How can we identify and characterize all species involved and their functional or pathological roles?
4. What are the structural and dynamic properties of IDPs in the protein-dense biomolecular condensates? How are their molecular properties linked to the functional roles of LLPS and to the mesoscopic behavior observed by rheology and microscopy?
5. How can we bridge the gap between the detailed biophysical investigation of well-defined reconstituted systems in vitro and the complex interactions and functions in vivo?

DISCLOSURE STATEMENT

The authors are not aware of any affiliations, memberships, funding, or financial holdings that might be perceived as affecting the objectivity of this review.

ACKNOWLEDGMENTS

We thank Jan-Philipp Günther, Miloš Ivanović, Oliver Stach, and Pedro Buzon Rodriguez for helpful comments on the manuscript. This work was supported by funding from the Swiss National Science Foundation (to B.S.) and the European Union's Horizon 2020 research and innovation program under Marie Skłodowska-Curie grant agreement 898228 (to A.C.).

LITERATURE CITED

1. Antonik M, Felekyan S, Gaiduk A, Seidel CAM. 2006. Separating structural heterogeneities from stochastic variations in fluorescence resonance energy transfer distributions via photon distribution analysis. *J. Phys. Chem. B* 110:6970–78

2. Asher WB, Geggier P, Holsey MD, Gilmore GT, Pati AK, et al. 2021. Single-molecule FRET imaging of GPCR dimers in living cells. *Nat. Methods* 18:397–405
3. Aubin JE. 1979. Autofluorescence of viable cultured mammalian cells. *J. Histochem. Cytochem.* 27:36–43
4. Avdoshenko SM, Das A, Satija R, Papoian GA, Makarov DE. 2017. Theoretical and computational validation of the Kuhn barrier friction mechanism in unfolded proteins. *Sci. Rep.* 7:269
5. Babu MM. 2016. The contribution of intrinsically disordered regions to protein function, cellular complexity, and human disease. *Biochem. Soc. Trans.* 44:1185–200
6. Bah A, Forman-Kay JD. 2016. Modulation of intrinsically disordered protein function by post-translational modifications. *J. Biol. Chem.* 291:6696–705
7. Banerjee PR, Mitrea DM, Kriwacki RW, Deniz AA. 2016. Asymmetric modulation of protein order–disorder transitions by phosphorylation and partner binding. *Angew. Chem. Int. Ed.* 55:1675–79
8. Banerjee PR, Moosa MM, Deniz AA. 2016. Two-dimensional crowding uncovers a hidden conformation of α-synuclein. *Angew. Chem. Int. Ed.* 55:12789–92
9. Benke S, Roderer D, Wunderlich B, Nettels D, Glockshuber R, Schuler B. 2015. The assembly dynamics of the cytolytic pore toxin ClyA. *Nat. Commun.* 6:6198
10. Berlow RB, Dyson HJ, Wright PE. 2017. Hypersensitive termination of the hypoxic response by a disordered protein switch. *Nature* 543:447–51
11. Berlow RB, Dyson HJ, Wright PE. 2018. Expanding the paradigm: intrinsically disordered proteins and allosteric regulation. *J. Mol. Biol.* 430:2309–20
12. Best RB. 2017. Computational and theoretical advances in studies of intrinsically disordered proteins. *Curr. Opin. Struct. Biol.* 42:147–54
13. Bigman LS, Iwahara J, Levy Y. 2022. Negatively charged disordered regions are prevalent and functionally important across proteomes. *J. Mol. Biol.* 434:167660
14. Boersma AJ, Zuhorn IS, Poolman B. 2015. A sensor for quantification of macromolecular crowding in living cells. *Nat. Methods* 12:227–29
15. Böhmer M, Wahl M, Rahn HJ, Erdmann R, Enderlein J. 2002. Time-resolved fluorescence correlation spectroscopy. *Chem. Phys. Lett.* 353:439–45
16. Borgia A, Borgia MB, Bugge K, Kissling VM, Heidarsson PO, et al. 2018. Extreme disorder in an ultrahigh-affinity protein complex. *Nature* 555:61–66
17. Borgia A, Zheng W, Buholzer K, Borgia MB, Schuler A, et al. 2016. Consistent view of polypeptide chain expansion in chemical denaturants from multiple experimental methods. *J. Am. Chem. Soc.* 138:11714–26
18. Bottaro S, Lindorff-Larsen K. 2018. Biophysical experiments and biomolecular simulations: a perfect match? *Science* 361:355–60
19. Brady JP, Farber PJ, Sekhar A, Lin YH, Huang R, et al. 2017. Structural and hydrodynamic properties of an intrinsically disordered region of a germ cell-specific protein on phase separation. *PNAS* 114:E8194–203
20. Brangwynne CP, Tompa P, Pappu RV. 2015. Polymer physics of intracellular phase transitions. *Nat. Phys.* 11:899–904
21. Bremer A, Farag M, Borcherds WM, Peran I, Martin EW, et al. 2022. Deciphering how naturally occurring sequence features impact the phase behaviours of disordered prion-like domains. *Nat. Chem.* 14:196–207
22. Bucciantini M, Giannoni E, Chiti F, Baroni F, Formigli L, et al. 2002. Inherent toxicity of aggregates implies a common mechanism for protein misfolding diseases. *Nature* 416:507–11
23. Budde J-H, van der Voort N, Felekyan S, Folz J, Kühnemuth R, et al. 2021. FRET nanoscopy enables seamless imaging of molecular assemblies with sub-nanometer resolution. arXiv:2108.00024 [physics.optics]
24. Burke KA, Janke AM, Rhine CL, Fawzi NL. 2015. Residue-by-residue view of in vitro FUS granules that bind the C-terminal domain of RNA polymerase II. *Mol. Cell* 60:231–41
25. Camacho-Zarco AR, Schnapka V, Guseva S, Abyzov A, Adamski W, et al. 2022. NMR provides unique insight into the functional dynamics and interactions of intrinsically disordered proteins. *Chem. Rev.* 122:9331–56
26. Chen TY, Cheng YS, Huang PS, Chen P. 2018. Facilitated unbinding via multivalency-enabled ternary complexes: new paradigm for protein-DNA interactions. *Acc. Chem. Res.* 51:860–68

27. Chowdhury A, Kovalenko SA, Aramburu IV, Tan PS, Ernsting NP, Lemke EA. 2019. Mechanism-dependent modulation of ultrafast interfacial water dynamics in intrinsically disordered protein complexes. *Angew. Chem. Int. Ed.* 58:4720–24
28. Chung HS, Eaton WA. 2018. Protein folding transition path times from single molecule FRET. *Curr. Opin. Struct. Biol.* 48:30–39
29. Chung HS, Louis JM, Gopich IV. 2016. Analysis of fluorescence lifetime and energy transfer efficiency in single-molecule photon trajectories of fast-folding proteins. *J. Phys. Chem. B* 120:680–99
30. Chung HS, Meng F, Kim JY, McHale K, Gopich IV, Louis JM. 2017. Oligomerization of the tetramerization domain of p53 probed by two- and three-color single-molecule FRET. *PNAS* 114:E6812–21
31. Crawford R, Torella JP, Aigrain L, Plochowietz A, Gryte K, et al. 2013. Long-lived intracellular single-molecule fluorescence using electroporated molecules. *Biophys. J.* 105:2439–50
32. Cremades N, Cohen SIA, Deas E, Abramov AY, Chen AY, et al. 2012. Direct observation of the interconversion of normal and toxic forms of α-synuclein. *Cell* 149:1048–59
33. Cubuk J, Alston JJ, Incicco JJ, Singh S, Stuchell-Brereton MD, et al. 2021. The SARS-CoV-2 nucleocapsid protein is dynamic, disordered, and phase separates with RNA. *Nat. Commun.* 12:1936
34. Das RK, Ruff KM, Pappu RV. 2015. Relating sequence encoded information to form and function of intrinsically disordered proteins. *Curr. Opin. Struct. Biol.* 32:102–12
35. de Torres J, Ghenuche P, Moparthi SB, Grigoriev V, Wenger J. 2015. FRET enhancement in aluminum zero-mode waveguides. *ChemPhysChem* 16:782–88
36. Demarest SJ, Martinez-Yamout M, Chung J, Chen H, Xu W, et al. 2002. Mutual synergistic folding in recruitment of CBP/p300 by p160 nuclear receptor coactivators. *Nature* 415:549–53
37. Dignon GL, Best RB, Mittal J. 2020. Biomolecular phase separation: from molecular driving forces to macroscopic properties. *Annu. Rev. Phys. Chem.* 71:53–75
38. Dingfelder F, Wunderlich B, Benke S, Zosel F, Zijlstra N, et al. 2017. Rapid microfluidic double-jump mixing device for single-molecule spectroscopy. *J. Am. Chem. Soc.* 139:6062–65
39. Doose S, Neuweiler H, Sauer M. 2009. Fluorescence quenching by photoinduced electron transfer: a reporter for conformational dynamics of macromolecules. *ChemPhysChem* 10:1389–98
40. Dyson HJ, Wright PE. 2021. NMR illuminates intrinsic disorder. *Curr. Opin. Struct. Biol.* 70:44–52
41. Eaton WA, Wolynes PG. 2017. Theory, simulations, and experiments show that proteins fold by multiple pathways. *PNAS* 114:E9759–60
42. Felekyan S, Kalinin S, Sanabria H, Valeri A, Seidel CAM. 2012. Filtered FCS: Species auto- and cross-correlation functions highlight binding and dynamics in biomolecules. *ChemPhysChem* 13:1036–53
43. Ferreon ACM, Ferreon JC, Wright PE, Deniz AA. 2013. Modulation of allostery by protein intrinsic disorder. *Nature* 498:390–94
44. Ferreon ACM, Gambin Y, Lemke EA, Deniz AA. 2009. Interplay of α-synuclein binding and conformational switching probed by single-molecule fluorescence. *PNAS* 106:5645–50
45. Fitzgerald GA, Terry DS, Warren AL, Quick M, Javitch JA, Blanchard SC. 2019. Quantifying secondary transport at single-molecule resolution. *Nature* 575:528–34
46. Follis AV, Llambi F, Merritt P, Chipuk JE, Green DR, Kriwacki RW. 2015. Pin1-induced proline isomerization in cytosolic p53 mediates BAX activation and apoptosis. *Mol. Cell* 59:677–84
47. Förster T. 1948. Zwischenmolekulare Energiewanderung und Fluoreszenz. *Ann. Phys.* 6:55–75
48. Frege T, Uversky VN. 2015. Intrinsically disordered proteins in the nucleus of human cells. *Biochem. Biophys. Rep.* 1:33–51
49. Fuxreiter M, Tompa P, eds. 2012. *Fuzziness: Structural Disorder in Protein Complexes*. Adv. Exp. Med. Biol. 725. Austin, TX: Landes Biosci.
50. Gambin Y, Vandelinder V, Ferreon AC, Lemke EA, Groisman A, Deniz AA. 2011. Visualizing a one-way protein encounter complex by ultrafast single-molecule mixing. *Nat. Methods* 8:239–41
51. George EM, Brown DT. 2010. Prothymosin alpha is a component of a linker histone chaperone. *FEBS Lett.* 584:2833–36
52. Gianni S, Dogan J, Jemth P. 2016. Coupled binding and folding of intrinsically disordered proteins: What can we learn from kinetics? *Curr. Opin. Struct. Biol.* 36:18–24

53. Gibbons RM. 1969. Scaled particle theory for particles of arbitrary shape. *Mol. Phys.* 17:81–86
54. Gibbs EB, Lu F, Portz B, Fisher MJ, Medellin BP, et al. 2017. Phosphorylation induces sequence-specific conformational switches in the RNA polymerase II C-terminal domain. *Nat. Commun.* 8:15233
55. Gomes GN, Gradinaru CC. 2017. Insights into the conformations and dynamics of intrinsically disordered proteins using single-molecule fluorescence. *Biochim. Biophys. Acta Proteins Proteom.* 1865:1696–706
56. Gopich IV, Szabo A. 2005. Theory of photon statistics in single-molecule Förster resonance energy transfer. *J. Chem. Phys.* 122:14707
57. Gopich IV, Szabo A. 2009. Decoding the pattern of photon colors in single-molecule FRET. *J. Phys. Chem. B* 113:10965–73
58. Gopich IV, Szabo A. 2012. Theory of the energy transfer efficiency and fluorescence lifetime distribution in single-molecule FRET. *PNAS* 109:7747–52
59. Gwosch KC, Pape JK, Balzarotti F, Hoess P, Ellenberg J, et al. 2020. MINFLUX nanoscopy delivers 3D multicolor nanometer resolution in cells. *Nat. Methods* 17:217–24
60. Heidarsson PO, Mercadante D, Sottini A, Nettels D, Borgia MB, et al. 2022. Release of linker histone from the nucleosome driven by polyelectrolyte competition with a disordered protein. *Nat. Chem.* 14:224–31
61. Hellenkamp B, Schmid S, Doroshenko O, Opanasyuk O, Kuhnemuth R, et al. 2018. Precision and accuracy of single-molecule FRET measurements—a multi-laboratory benchmark study. *Nat. Methods* 15:669–76
62. Hellenkamp B, Thurn J, Stadlmeier M, Hugel T. 2018. Kinetics of transient protein complexes determined via diffusion-independent microfluidic mixing and fluorescence stoichiometry. *J. Phys. Chem. B* 122:11554–60
63. Hergeth SP, Schneider R. 2015. The H1 linker histones: multifunctional proteins beyond the nucleosomal core particle. *EMBO Rep.* 16:1439–53
64. Hillger F, Hänni D, Nettels D, Geister S, Grandin M, et al. 2008. Probing protein-chaperone interactions with single molecule fluorescence spectroscopy. *Angew. Chem. Int. Ed.* 47:6184–88
65. Hines KE, Bankston JR, Aldrich RW. 2015. Analyzing single-molecule time series via nonparametric Bayesian inference. *Biophys. J.* 108:540–56
66. Hoffer NQ, Woodside MT. 2019. Probing microscopic conformational dynamics in folding reactions by measuring transition paths. *Curr. Opin. Chem. Biol.* 53:68–74
67. Hoffmann A, Kane A, Nettels D, Hertzog DE, Baumgärtel P, et al. 2007. Mapping protein collapse with single-molecule fluorescence and kinetic synchrotron radiation circular dichroism spectroscopy. *PNAS* 104:105–10
68. Holmstrom ED, Holla A, Zheng W, Nettels D, Best RB, Schuler B. 2018. Accurate transfer efficiencies, distance distributions, and ensembles of unfolded and intrinsically disordered proteins from single-molecule FRET. *Methods Enzymol.* 611:287–325
69. Holmstrom ED, Liu ZW, Nettels D, Best RB, Schuler B. 2019. Disordered RNA chaperones can enhance nucleic acid folding via local charge screening. *Nat. Commun.* 10:2453
70. Hwang H, Myong S. 2014. Protein induced fluorescence enhancement (PIFE) for probing protein–nucleic acid interactions. *Chem. Soc. Rev.* 43:1221–29
71. Iljina M, Garcia GA, Horrocks MH, Tosatto L, Choi ML, et al. 2016. Kinetic model of the aggregation of α-synuclein provides insights into prion-like spreading. *PNAS* 113:E1206–15
72. Juette MF, Terry DS, Wasserman MR, Altman RB, Zhou Z, et al. 2016. Single-molecule imaging of non-equilibrium molecular ensembles on the millisecond timescale. *Nat. Methods* 13:341–44
73. Kalinin S, Valeri A, Antonik M, Felekyan S, Seidel CA. 2010. Detection of structural dynamics by FRET: a photon distribution and fluorescence lifetime analysis of systems with multiple states. *J. Phys. Chem. B* 114:7983–95
74. Kang H, Pincus PA, Hyeon C, Thirumalai D. 2015. Effects of macromolecular crowding on the collapse of biopolymers. *Phys. Rev. Lett.* 114:068303
75. Kapanidis AN, Laurence TA, Lee NK, Margeat E, Kong X, Weiss S. 2005. Alternating-laser excitation of single molecules. *Acc. Chem. Res.* 38:523–33

76. Kar M, Dar F, Welsh TJ, Vogel LT, Kuhnemuth R, et al. 2022. Phase-separating RNA-binding proteins form heterogeneous distributions of clusters in subsaturated solutions. *PNAS* 119:e2202222119
77. Kikhney AG, Svergun DI. 2015. A practical guide to small angle X-ray scattering (SAXS) of flexible and intrinsically disordered proteins. *FEBS Lett.* 589:2570–77
78. Kim JY, Chung HS. 2020. Disordered proteins follow diverse transition paths as they fold and bind to a partner. *Science* 368:1253–57
79. Kim JY, Meng F, Yoo J, Chung HS. 2018. Diffusion-limited association of disordered protein by non-native electrostatic interactions. *Nat. Commun.* 9:4707
80. Kim PS, Baldwin RL. 1982. Specific intermediates in the folding reactions of small proteins and the mechanism of protein folding. *Annu. Rev. Biochem.* 51:459–89
81. Klose D, Holla A, Gmeiner C, Nettels D, Ritsch I, et al. 2021. Resolving distance variations by single-molecule FRET and EPR spectroscopy using rotamer libraries. *Biophys. J.* 120:4842–58
82. Knight JB, Vishwanath A, Brody JP, Austin RH. 1998. Hydrodynamic focusing on a silicon chip: mixing nanoliters in microseconds. *Phys. Rev. Lett.* 80:3863–66
83. König I, Soranno A, Nettels D, Schuler B. 2021. Impact of in-cell and in-vitro crowding on the conformations and dynamics of an intrinsically disordered protein. *Angew. Chem. Int. Ed.* 60:10724–29
84. König I, Zarrine-Afsar A, Aznauryan M, Soranno A, Wunderlich B, et al. 2015. Single-molecule spectroscopy of protein conformational dynamics in live eukaryotic cells. *Nat. Methods* 12:773–79
85. Kudryavtsev V, Sikor M, Kalinin S, Mokranjac D, Seidel CAM, Lamb DC. 2012. Combining MFD and PIE for accurate single-pair Förster resonance energy transfer measurements. *ChemPhysChem* 13:1060–78
86. Lakowicz JR. 1999. *Principles of Fluorescence Spectroscopy*. New York: Kluwer Acad.
87. Lamboy JA, Kim H, Lee KS, Ha T, Komives EA. 2011. Visualization of the nanospring dynamics of the IκBα ankyrin repeat domain in real time. *PNAS* 108:10178–83
88. LeBlanc SJ, Kulkarni P, Weninger KR. 2018. Single molecule FRET: a powerful tool to study intrinsically disordered proteins. *Biomolecules* 8:140
89. Lee NK, Kapanidis AN, Wang Y, Michalet X, Mukhopadhyay J, et al. 2005. Accurate FRET measurements within single diffusing biomolecules using alternating-laser excitation. *Biophys. J.* 88:2939–53
90. Leisle L, Chadda R, Lueck JD, Infield DT, Galpin JD, et al. 2016. Cellular encoding of Cy dyes for single-molecule imaging. *eLife* 5:e19088
91. Lerner E, Barth A, Hendrix J, Ambrose B, Birkedal V, et al. 2021. FRET-based dynamic structural biology: challenges, perspectives and an appeal for open-science practices. *eLife* 10:e60416
92. Li J, Hilser VJ. 2018. Assessing allostery in intrinsically disordered proteins with ensemble allosteric model. *Methods Enzymol.* 611:531–57
93. Lipman EA, Schuler B, Bakajin O, Eaton WA. 2003. Single-molecule measurement of protein folding kinetics. *Science* 301:1233–35
94. Martin EW, Holehouse AS, Peran I, Farag M, Incicco JJ, et al. 2020. Valence and patterning of aromatic residues determine the phase behavior of prion-like domains. *Science* 367:694–99
95. McKibben KM, Rhoades E. 2019. Independent tubulin binding and polymerization by the proline-rich region of Tau is regulated by Tau's N-terminal domain. *J. Biol. Chem.* 294:19381–94
96. McKinney SA, Joo C, Ha T. 2006. Analysis of single-molecule FRET trajectories using hidden Markov modeling. *Biophys. J.* 91:1941–51
97. Melo AM, Coraor J, Alpha-Cobb G, Elbaum-Garfinkle S, Nath A, Rhoades E. 2016. A functional role for intrinsic disorder in the tau-tubulin complex. *PNAS* 113:14336–41
98. Meng F, Yoo J, Chung HS. 2022. Single-molecule fluorescence imaging and deep learning reveal highly heterogeneous aggregation of amyloid-beta 42. *PNAS* 119:e2116736119
99. Metskas LA, Rhoades E. 2020. Single-molecule FRET of intrinsically disordered proteins. *Annu. Rev. Phys. Chem.* 71:391–414
100. Milles S, Huy Bui K, Koehler C, Eltsov M, Beck M, Lemke EA. 2013. Facilitated aggregation of FG nucleoporins under molecular crowding conditions. *EMBO Rep.* 14:178–83
101. Milles S, Mercadante D, Aramburu IV, Jensen MR, Banterle N, et al. 2015. Plasticity of an ultrafast interaction between nucleoporins and nuclear transport receptors. *Cell* 163:734–45

102. Mitrea DM, Cika JA, Guy CS, Ban D, Banerjee PR, et al. 2016. Nucleophosmin integrates within the nucleolus via multi-modal interactions with proteins displaying R-rich linear motifs and rRNA. *eLife* 5:e13571
103. Mitrea DM, Cika JA, Stanley CB, Nourse A, Onuchic PL, et al. 2018. Self-interaction of NPM1 modulates multiple mechanisms of liquid-liquid phase separation. *Nat. Commun.* 9:842
104. Mittag T, Forman-Kay JD. 2007. Atomic-level characterization of disordered protein ensembles. *Curr. Opin. Struct. Biol.* 17:3–14
105. Mittag T, Marsh J, Grishaev A, Orlicky S, Lin H, et al. 2010. Structure/function implications in a dynamic complex of the intrinsically disordered Sic1 with the Cdc4 subunit of an SCF ubiquitin ligase. *Structure* 18:494–506
106. Morger D, Zosel F, Buhlmann M, Zuger S, Mittelviefhaus M, et al. 2018. The three-fold axis of the HIV-1 capsid lattice is the species-specific binding interface for TRIM5α. *J. Virol.* 92:e01541-17
107. Nasir I, Onuchic PL, Labra SR, Deniz AA. 2019. Single-molecule fluorescence studies of intrinsically disordered proteins and liquid phase separation. *Biochim. Biophys. Acta Proteins Proteom.* 1867:980–87
108. Nath A, Sammalkorpi M, DeWitt DC, Trexler AJ, Elbaum-Garfinkle S, et al. 2012. The conformational ensembles of α-synuclein and tau: combining single-molecule FRET and simulations. *Biophys. J.* 103:1940–49
109. Nettels D, Gopich IV, Hoffmann A, Schuler B. 2007. Ultrafast dynamics of protein collapse from single-molecule photon statistics. *PNAS* 104:2655–60
110. Nir E, Michalet X, Hamadani KM, Laurence TA, Neuhauser D, et al. 2006. Shot-noise limited single-molecule FRET histograms: comparison between theory and experiments. *J. Phys. Chem. B* 110:22103–24
111. Nüesch MF, Ivanovic MT, Claude JB, Nettels D, Best RB, et al. 2022. Single-molecule detection of ultrafast biomolecular dynamics with nanophotonics. *J. Am. Chem. Soc.* 144:52–56
112. Oates ME, Romero P, Ishida T, Ghalwash M, Mizianty MJ, et al. 2013. D^2P^2: database of disordered protein predictions. *Nucleic Acids Res.* 41:D508–16
113. O'Brien EP, Morrison G, Brooks BR, Thirumalai D. 2009. How accurate are polymer models in the analysis of Förster resonance energy transfer experiments on proteins? *J. Chem. Phys.* 130:124903
114. Oldfield CJ, Meng J, Yang JY, Yang MQ, Uversky VN, Dunker AK. 2008. Flexible nets: disorder and induced fit in the associations of p53 and 14-3-3 with their partners. *BMC Genom.* 9(Suppl. 1):S1
115. Olsen JG, Teilum K, Kragelund BB. 2017. Behaviour of intrinsically disordered proteins in protein-protein complexes with an emphasis on fuzziness. *Cell. Mol. Life Sci.* 74:3175–83
116. Orte A, Birkett NR, Clarke RW, Devlin GL, Dobson CM, Klenerman D. 2008. Direct characterization of amyloidogenic oligomers by single-molecule fluorescence. *PNAS* 105:14424–29
117. Patterson G, Davidson M, Manley S, Lippincott-Schwartz J. 2010. Superresolution imaging using single-molecule localization. *Annu. Rev. Phys. Chem.* 61:345–67
118. Peng B, Muthukumar M. 2015. Modeling competitive substitution in a polyelectrolyte complex. *J. Chem. Phys.* 143:243133
119. Peng S, Sun R, Wang W, Chen C. 2017. Single-molecule photoactivation FRET: a general and easy-to-implement approach to break the concentration barrier. *Angew. Chem. Int. Ed.* 56:6882–85
120. Pfeil SH, Wickersham CE, Hoffmann A, Lipman EA. 2009. A microfluidic mixing system for single-molecule measurements. *Rev. Sci. Instrum.* 80:055105
121. Phillips AH, Kriwacki RW. 2020. Intrinsic protein disorder and protein modifications in the processing of biological signals. *Curr. Opin. Struct. Biol.* 60:1–6
122. Pinotsi D, Buell AK, Galvagnion C, Dobson CM, Kaminski Schierle GS, Kaminski CF. 2014. Direct observation of heterogeneous amyloid fibril growth kinetics via two-color super-resolution microscopy. *Nano Lett.* 14:339–45
123. Plitzko JM, Schuler B, Selenko P. 2017. Structural biology outside the box—inside the cell. *Curr. Opin. Struct. Biol.* 46:110–21
124. Rajagopalan S, Huang F, Fersht AR. 2011. Single-molecule characterization of oligomerization kinetics and equilibria of the tumor suppressor p53. *Nucleic Acids Res.* 39:2294–303

125. Ruff KM, Pappu RV, Holehouse AS. 2019. Conformational preferences and phase behavior of intrinsically disordered low complexity sequences: insights from multiscale simulations. *Curr. Opin. Struct. Biol.* 56:1–10
126. Sakmann B, Neher E. 1995. *Single Channel Recording*. New York: Plenum Press
127. Sakon JJ, Weninger KR. 2010. Detecting the conformation of individual proteins in live cells. *Nat. Methods* 7:203–5
128. Sarkar M, Smith AE, Pielak GJ. 2013. Impact of reconstituted cytosol on protein stability. *PNAS* 110:19342–47
129. Schreiber G, Haran G, Zhou HX. 2009. Fundamental aspects of protein-protein association kinetics. *Chem. Rev.* 109:839–60
130. Schuler B. 2013. Single-molecule FRET of protein structure and dynamics—a primer. *J. Nanobiotechnol.* 11(Suppl. 1):S2
131. Schuler B. 2018. Perspective: chain dynamics of unfolded and intrinsically disordered proteins from nanosecond fluorescence correlation spectroscopy combined with single-molecule FRET. *J. Chem. Phys.* 149:010901
132. Schuler B, Borgia A, Borgia MB, Heidarsson PO, Holmstrom ED, et al. 2020. Binding without folding—the biomolecular function of disordered polyelectrolyte complexes. *Curr. Opin. Struct. Biol.* 60:66–76
133. Schuler B, Lipman EA, Steinbach PJ, Kumke M, Eaton WA. 2005. Polyproline and the "spectroscopic ruler" revisited with single molecule fluorescence. *PNAS* 102:2754–59
134. Schuler B, Soranno A, Hofmann H, Nettels D. 2016. Single-molecule FRET spectroscopy and the polymer physics of unfolded and intrinsically disordered proteins. *Annu. Rev. Biophys.* 45:207–31
135. Seim I, Posey AE, Snead WT, Stormo BM, Klotsa D, et al. 2022. Dilute phase oligomerization can oppose phase separation and modulate material properties of a ribonucleoprotein condensate. *PNAS* 119:e2120799119
136. Selvin PR, Ha T. 2008. *Single-Molecule Techniques: A Laboratory Manual*. New York: Cold Spring Harb. Lab. Press
137. Sgouralis I, Madaan S, Djutanta F, Kha R, Hariadi RF, Presse S. 2019. A Bayesian nonparametric approach to single molecule Förster resonance energy transfer. *J. Phys. Chem. B* 123:675–88
138. Shammas SL, Crabtree MD, Dahal L, Wicky BI, Clarke J. 2016. Insights into coupled folding and binding mechanisms from kinetic studies. *J. Biol. Chem.* 291:6689–95
139. Shammas SL, Garcia GA, Kumar S, Kjaergaard M, Horrocks MH, et al. 2015. A mechanistic model of tau amyloid aggregation based on direct observation of oligomers. *Nat. Commun.* 6:7025
140. Shea JE, Best RB, Mittal J. 2021. Physics-based computational and theoretical approaches to intrinsically disordered proteins. *Curr. Opin. Struct. Biol.* 67:219–25
141. Shoemaker BA, Portman JJ, Wolynes PG. 2000. Speeding molecular recognition by using the folding funnel: the fly-casting mechanism. *PNAS* 97:8868–73
142. Sisamakis E, Valeri A, Kalinin S, Rothwell PJ, Seidel CAM. 2010. Accurate single-molecule FRET studies using multiparameter fluorescence detection. *Methods Enzymol.* 475:455–514
143. Smyth S, Zhang Z, Bah A, Tsangaris TE, Dawson J, et al. 2022. Multisite phosphorylation and binding alter conformational dynamics of the 4E-BP2 protein. *Biophys. J.* 121:3049–60
144. Soranno A, Buchli B, Nettels D, Müller-Späth S, Cheng RR, et al. 2012. Quantifying internal friction in unfolded and intrinsically disordered proteins with single molecule spectroscopy. *PNAS* 109:17800–6
145. Soranno A, Holla A, Dingfelder F, Nettels D, Makarov DE, Schuler B. 2017. Integrated view of internal friction in unfolded proteins from single-molecule FRET, contact quenching, theory, and simulations. *PNAS* 114:E1833–39
146. Soranno A, König I, Borgia MB, Hofmann H, Zosel F, et al. 2014. Single-molecule spectroscopy reveals polymer effects of disordered proteins in crowded environments. *PNAS* 111:4874–79
147. Soranno A, Zosel F, Hofmann H. 2018. Internal friction in an intrinsically disordered protein—comparing Rouse-like models with experiments. *J. Chem. Phys.* 148:123326
148. Sottini A, Borgia A, Borgia MB, Bugge K, Nettels D, et al. 2020. Polyelectrolyte interactions enable rapid association and dissociation in high affinity disordered protein complexes. *Nat. Commun.* 11:5736
149. Stadler AM, Stingaciu L, Radulescu A, Holderer O, Monkenbusch M, et al. 2014. Internal nanosecond dynamics in the intrinsically disordered myelin basic protein. *J. Am. Chem. Soc.* 136:6987–94

150. Stracy M, Kapanidis AN. 2017. Single-molecule and super-resolution imaging of transcription in living bacteria. *Methods* 120:103–14
151. Stryer L, Haugland RP. 1967. Energy transfer: a spectroscopic ruler. *PNAS* 58:719–26
152. Stuchell-Brereton MD, Zimmerman MI, Miller JJ, Mallimadugula UL, Incicco JJ, et al. 2023. Apolipoprotein E4 has extensive conformational heterogeneity in lipid-free and lipid-bound forms. *PNAS* 120:e2215371120
153. Sturzenegger F, Zosel F, Holmstrom ED, Buholzer KJ, Makarov DE, et al. 2018. Transition path times of coupled folding and binding reveal the formation of an encounter complex. *Nat. Commun.* 9:4708
154. Szalai AM, Siarry B, Lukin J, Giusti S, Unsain N, et al. 2021. Super-resolution imaging of energy transfer by intensity-based STED-FRET. *Nano Lett.* 21:2296–303
155. Tan PS, Aramburu IV, Mercadante D, Tyagi S, Chowdhury A, et al. 2018. Two differential binding mechanisms of FG-nucleoporins and nuclear transport receptors. *Cell Rep.* 22:3660–71
156. Theillet FX, Kalmar L, Tompa P, Han KH, Selenko P, et al. 2013. The alphabet of intrinsic disorder: I. Act like a Pro: on the abundance and roles of proline residues in intrinsically disordered proteins. *Intrinsically Disord. Proteins* 1:e24360
157. Thomasen FE, Lindorff-Larsen K. 2022. Conformational ensembles of intrinsically disordered proteins and flexible multidomain proteins. *Biochem. Soc. Trans.* 50:541–54
158. Tompa P, Fuxreiter M. 2008. Fuzzy complexes: polymorphism and structural disorder in protein-protein interactions. *Trends Biochem. Sci.* 33:2–8
159. Trexler AJ, Rhoades E. 2009. α-Synuclein binds large unilamellar vesicles as an extended helix. *Biochemistry* 48:2304–6
160. Tsang B, Pritisanac I, Scherer SW, Moses AM, Forman-Kay JD. 2020. Phase separation as a missing mechanism for interpretation of disease mutations. *Cell* 183:1742–56
161. Tsytlonok M, Sanabria H, Wang Y, Felekyan S, Hemmen K, et al. 2019. Dynamic anticipation by Cdk2/Cyclin A-bound p27 mediates signal integration in cell cycle regulation. *Nat. Commun.* 10:1676
162. van der Lee R, Buljan M, Lang B, Weatheritt RJ, Daughdrill GW, et al. 2014. Classification of intrinsically disordered regions and proteins. *Chem. Rev.* 114:6589–631
163. Vancraenenbroeck R, Harel YS, Zheng W, Hofmann H. 2019. Polymer effects modulate binding affinities in disordered proteins. *PNAS* 116:19506–12
164. Veldhuis G, Segers-Nolten I, Ferlemann E, Subramaniam V. 2009. Single-molecule FRET reveals structural heterogeneity of SDS-bound α-synuclein. *ChemBioChem* 10:436–39
165. Weickert S, Cattani J, Drescher M. 2019. Intrinsically disordered proteins (IDPs) studied by EPR and in-cell EPR. In *Electron Paramagnetic Resonance*, Vol. 26, pp. 1–37. London: R. Soc. Chem.
166. Wen J, Hong L, Krainer G, Yao Q-Q, Knowles TPJ, et al. 2021. Conformational expansion of Tau in condensates promotes irreversible aggregation. *J. Am. Chem. Soc.* 143:13056–64
167. Wiggers F, Wohl S, Dubovetskyi A, Rosenblum G, Zheng W, Hofmann H. 2021. Diffusion of a disordered protein on its folded ligand. *PNAS* 118:e2106690118
168. Wright PE, Dyson HJ. 2009. Linking folding and binding. *Curr. Opin. Struct. Biol.* 19:31–38
169. Wright PE, Dyson HJ. 2015. Intrinsically disordered proteins in cellular signalling and regulation. *Nat. Rev. Mol. Cell Biol.* 16:18–29
170. Wunderlich B, Nettels D, Benke S, Clark J, Weidner S, et al. 2013. Microfluidic mixer designed for performing single-molecule kinetics with confocal detection on timescales from milliseconds to minutes. *Nat. Protoc.* 8:1459–74
171. Zbinden A, Perez-Berlanga M, De Rossi P, Polymenidou M. 2020. Phase separation and neurodegenerative diseases: a disturbance in the force. *Dev. Cell* 55:45–68
172. Zheng W, Hofmann H, Schuler B, Best RB. 2018. Origin of internal friction in disordered proteins depends on solvent quality. *J. Phys. Chem. B* 122:11478–87
173. Zheng W, Zerze GH, Borgia A, Mittal J, Schuler B, Best RB. 2018. Inferring properties of disordered chains from FRET transfer efficiencies. *J. Chem. Phys.* 148:123329
174. Zhou HX, Rivas GN, Minton AP. 2008. Macromolecular crowding and confinement: biochemical, biophysical, and potential physiological consequences. *Annu. Rev. Biophys.* 37:375–97
175. Zhu P, Craighead HG. 2012. Zero-mode waveguides for single-molecule analysis. *Annu. Rev. Biophys.* 41:269–93

176. Zijlstra N, Dingfelder F, Wunderlich B, Zosel F, Benke S, et al. 2017. Rapid microfluidic dilution for single-molecule spectroscopy of low-affinity biomolecular complexes. *Angew. Chem. Int. Ed.* 56:7126–29
177. Zimmerman SB, Trach SO. 1991. Estimation of macromolecule concentrations and excluded volume effects for the cytoplasm of *Escherichia coli*. *J. Mol. Biol.* 222:599–620
178. Ziv G, Thirumalai D, Haran G. 2009. Collapse transition in proteins. *Phys. Chem. Chem. Phys.* 11:83–93
179. Zosel F, Holla A, Schuler B. 2022. Labeling of proteins for single-molecule fluorescence spectroscopy. *Methods Mol. Biol.* 2376:207–33
180. Zosel F, Mercadante D, Nettels D, Schuler B. 2018. A proline switch explains kinetic heterogeneity in a coupled folding and binding reaction. *Nat. Commun.* 9:3332
181. Zosel F, Soranno A, Buholzer KJ, Nettels D, Schuler B. 2020. Depletion interactions modulate the binding between disordered proteins in crowded environments. *PNAS* 117:13480–89

Annual Review of Biophysics
Volume 52, 2023

Contents

Indexes

Errata

An online log of corrections to *Annual Review of Biophysics* articles may be found at http://www.annualreviews.org/errata/biophys